CHAPTER 4

DESIGN AND PIC SIMULATION OF THE FEL AMPLIFIERS

*Part of this work has been published as:

Ram Gopal and P. K. Jain, "Design methodology and simulation study of a free electron laser amplifier", *International Journal of Engineering & Technology*, Vol. 7, No. 4, pp. 3175-3181, 2018.

CHAPTER 4

DESIGN AND PIC SIMULATION OF THE FEL AMPLIFIERS

4.1. Introduction

The device, FEL amplifiers (FELA) has been developed using an intense relativistic electron beams (IREBs) with zero percent velocity spreading and $1-2MeV$ moderating energy [Gold *et al.* (1984), Pant and Tripathi (1994)]. It is demonstrated for extremely high power, continuous tunable radiation and moderated efficiency of the source in sub millimeter to optical ranges and the potential application in the field of communication system, nuclear fusion, radio astronomy, military applications, atmospheric studies, chemical and isotope separation, inertial confinement fusion, remote sensing and security identification, plasma accelerator diagnostics, medicine and molecular spectroscopy, biological imaging (general test, measurement and diagnosis), room temperature THz imaging, materials characterization (spectroscopy of solids and liquids), build computer chips and to clean up toxic waste, electronic material processing, nanotubes synthesis and many other curriculums [Liu and Tripathi (1994), Jia (2011), Pae and Hahn (2002), Shea and Fruend (2001), Pellegrini (1990), Pellegrini and Reiche (2004)]. The operating radiation frequency of FEL amplifiers λ_1 scales with wiggler period λ_o and beam Lorentz factor or the relativistic gamma factor (γ_o) of the electron beam, $\gamma_o = 1 + E_b / mc^2$ as $\lambda_1 = \lambda_0 / 2\gamma_o^{\,2}$ where E_b is the beam kinetic energy, m is the rest mass of electrons and c is the light velocity in vacuum and the synchronous bunching and phase matching phenomenon to be satisfied as $\omega = \omega_1 - \omega_o$ and $k = k_o + k_1$ [Liu and Tripathi (1994),

Sharma and Tripathi (1996), Pant and Tripathi (1994)]. The primary importance of the device is essential for operating behavior and optimization in the TM_{01} and extraction of the RF output from the electron beams. Although the radiated signal is tuned by very small wiggler period and/or higher electron beams energy or ambient magnetic fields, however, in practically, it is not accessible more easily for high beams energy as well as shortening the wiggler periods and also typically, not all, the magnetic wiggler field are not easily accessible for very small wiggler wavelengths [Gopal and Jain (2018), Gopal and Jain (2018), Motz (1951), Sharma and Tripathi (1993), Sharma and Tripathi (1996)].

The typical layout and 3-D schematic diagram of the FEL amplifier is shown in below Fig. 4.1, which consists electron gun and accelerator, bitter magnets/axial field coils, wiggler magnets/undulator, depressed collector for beam dumped, beam interaction chamber, electron beams and optical mirror for radiated output of the FEL amplifiers. An electron gun is the first component. The accelerator, which generated a suitable voltage $> 500kV$ (it is very high as $1GV$) and current ($>1A$ to $100kA$) for the electron beams but it have some limitations. It is approximated $17kA$ [Marshall (1985), Liu and Tripathi (1994)]. Normally the pulse duration is used $\leq 100n\sec$ for the beams while $\approx 1m\sec$ are also used in some other experiments. The hot or cold cathode provided electrons acceleration through the diode structure together with the strong axial guided magnetic field and/or focusing elements. Here the FEL amplifier frequency radiation underlets on γ_{ob}^{o} (relativistic gamma factor) while, approximate 0.1% spread energy of the electron beams and the radius of the beams $1cm$ with $\approx 1-2mm$ beams thickness. Typically, the approximate values of the wiggler strengths is $\approx 1kG$ and the magnetic wiggler wavelengths

$\approx 3cm$ [Liu and Tripathi (1994)]. The tapered wiggler with magnitude B_o and the period of the wiggler $2\pi / k_o$ have adiabatically changes along the FEL amplifier structure with slowing down the beat-wave, hence, the linear tapered axial magnetic fields leading to improve the efficiency of the amplifier also.

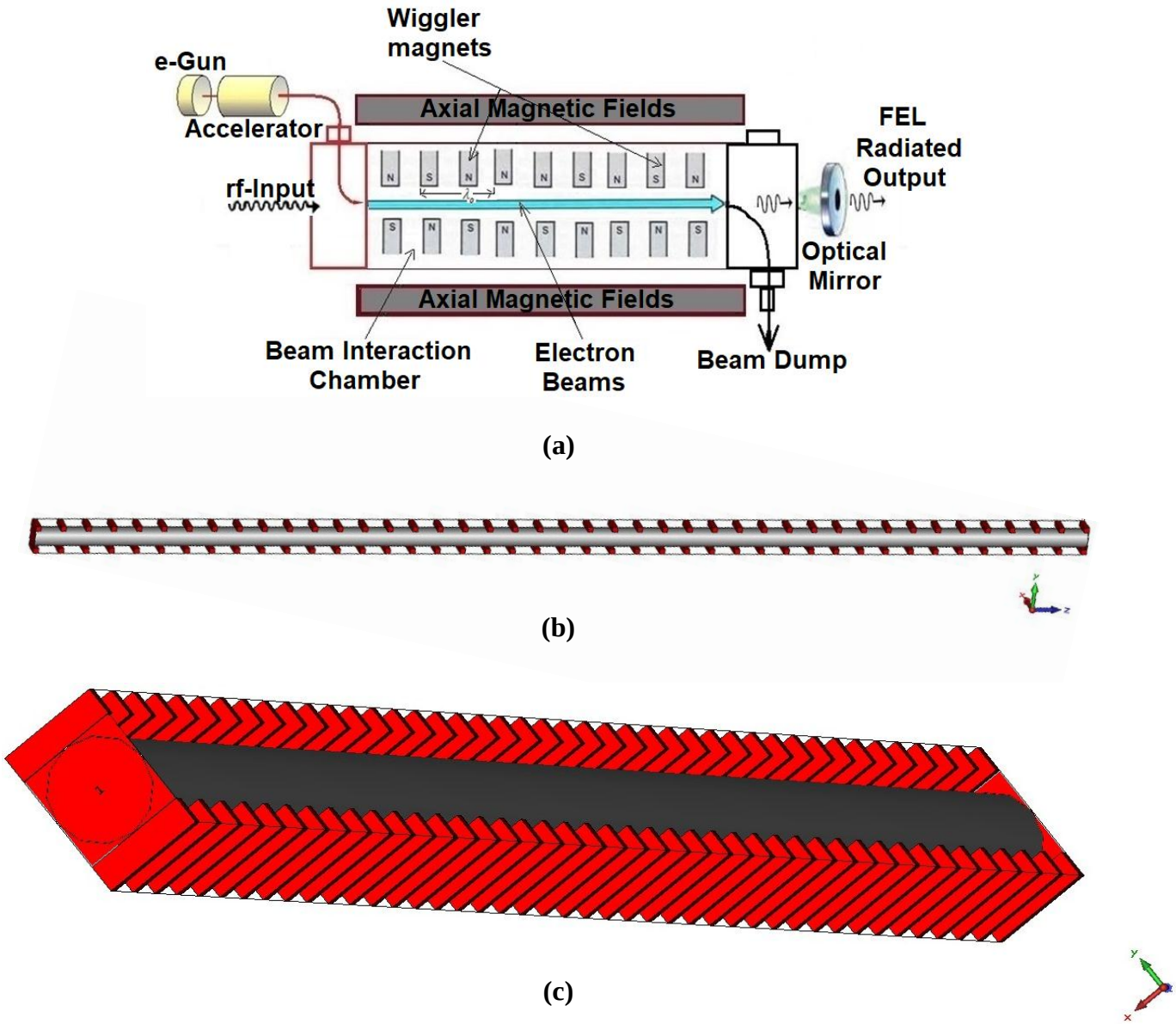

Figure 4.1: Typical layout [Gopal and Jain (2018)] (a) and 3-D schematic diagram for simulation of the FEL amplifiers (b & c) [Gopal and Jain (2018)].

FEL amplifiers have a high broad band reflecting mirror at output. The recovery of energy is another important issue of the beams spent into the interaction chamber and collected at the output port through the depressed collectors and ignoring here, boundary effects for FEL amplifier growth rate radiated into the interaction chamber [Roberson and Sprangle (1989), Dattoli, Renieri and Torre (1993), Workie (2001)].

The basic design consideration and challenges of FEL amplifiers simulation codes have become an integral part of the design of new devices and the analysis and diagnosis of existing machines. The three-dimensional simulation and experiment code GENESIS [Reiche (1999)] was used for the Linac Coherent Light Source (LCLS) at 1.5 Å measured power for the closed agreement demonstration while TDA [Tran and Wurtele (1989)] used as the steady-state particle simulation codes seeded by a monochromatic external radiation field. GINGER, GENESIS and SIMPLEX are the "time-dependent" simulation codes used in steady-state mode also [Fawley (2002), Reiche (1999) and Tanaka (2004)]. The time-dependent code ALICE implements open boundary conditions for the paraxial wave equation [Zagorornov and Dohlus (2009)] while an integral representation of the paraxial wave equation is used in RON [Dejus, Shevchenko and Vinokurov (1999)] and FAST [Saldin, Schneidmiller and Yurkov (1999)]. All of the above codes are based on the wiggler-period-averaged FEL equations, which assume the field develops slowly over many undulator periods. A non-wiggler-averaged code, MEDUSA has been developed to include higher harmonics from the beginning [Freund, Biedron and Milton (2000)]. Finally, several codes are well-developed for realistic FEL simulations, especially for single-pass, high-gain systems. Last but not least, these advanced codes are also improved the ability to take input from and give output to accelerator tracking codes such as ELEGANT/IMPACT

[Borland, (2000)]. While certain particle data has been exchanged to perform start-to-end FEL simulations, improved interfaces is more readily handle the transfer the microscopic beam distribution.

The facilities of the designation of high power microwave (HPM) devices and the description of the mechanism between beam-wave interactions, there are several modeling and simulation techniques has been reported. The MAGY, ARGUS and CHICPIC, there are many numerical techniques based simulation codes are employed successfully for the electromagnetic behavior of the amplifier, commercially, it is not easily available but only used for the design optimization and their validation of the device [Nguyen *et al.* (2000), Petillo *et al.* (1993), Di, Zhu and Liu (2005)]. The MAGIC, "particle-in-cell (PIC) simulation codes" has been envansigated to examine the FEL amplifier successfully and also applicable to use for commercially [Warren *et al.* (1993), MAGIC User's Manual (2007)]. The computer simulation technology (CST) particle studio, PIC simulation codes is another advanced technique to studied the finite integration methods and exhibition of the possibilities of main mode temporal growth [*User's Manual*, CST-Particle Studio (2013), *User's Manual*, CST-Particle Studio (2014), Kartikeyan, Borie and Thumn (2004), Nusinovich (2004), Swati, Chauhan and Jain (2016), Mahto and Jain (2016)].

In the recent and presented work, the simulation and design methodology through particle-in-cell (PIC) simulation codes of the FEL amplifiers by emissions of electrons, comprehensive are not reported. Here we examine an explosive derivation to start the amplifier oscillation and derived the design methodology of the device. The emission process in the FEL amplifiers (FELA) interaction chamber is simulated through the commercially 3-D PIC simulation codes "CST Particle Studio". To find out the excitation

of electromagnetic modes, frequencies and EM field patterns inside the interaction region of an amplifier is carried out through the Eigen mode simulation (i.e., cold simulation or beams absent simulations). To observed the overall performance of an FEL amplifiers, such as frequency of operations, gain, power, efficiency, RF output and the beams present PIC simulation is carried out.

In this chapter 4, the following organizations of the thesis work are presented. The consideration of design parameter is discussed in Section 4.2. The RF interaction modeling, Eigen mode simulation and parametric analysis are described in section 4.3 and in their subsections 4.3.1, 4.3.2 and 4.3.3, which is compared with the earlier reported experimental values [Gold *et al.* (1984), Gold *et al.* (1984), Gold *et al.* (1987), Pant and Tripathi (1994)]. Further, the conclusion of the device PIC simulation in CST particle studio to validate the parametric analysis is drawn in section 4.4.

4.2. Device Design Methodology

There are major rigorous to design of free electron laser amplifiers (FELA) at higher frequencies for the various parameters. The process of proper designing of FEL amplifiers is required to ensure the RF interaction structure, helical wiggler, drift tube with desired operating mode, mode of extraction, frequency operation, electron beam parameter, high output power, moderate efficiency, axial fields, magnetic fields and so on. The beam current and voltage chosen initially through the selection procedure of the desired power output, extraction efficiency and the beams electron space charge effect. Typically, the TM_{01} mode is selected for the operating behavior of an amplifier and their dimensions of RF interaction structure, the beam parameters (i.e., velocity spreading ratio $\leq 0.1\%$ and the

guiding radius), modulating interaction radius, wiggler field and strong axial magnetic field are estimated to established analysis [Freund and Antonsen, Jr. (2018), Marshall (1985), Liu and Tripathi (1994), Tripathi (2013), Kartikeyan, Borie and Thumn (2004), Nusinovich (2004), Swati, Chauhan and Jain (2016)]. The amplifier design modeling of beam radius, drift tube radius and wiggler periods etc. are given below in details.

4.2.1. Drift tube, beam radius and wiggler modeling

If the FEL amplifiers are operated in the TM_{mn} mode and the radius of the drift tube for cylindrical wave guide into the interaction chamber of FEL amplifiers is R_{dt-FEL}, then the expression [Freund and Antonsen, Jr. (2018), Swati, Chauhan and Jain (2016)] is as-

$$R_{dt-FEL} = \frac{\chi'_{mn}}{k'_{mn}} = \frac{\chi'_{mn} c}{2\pi f'_c} \tag{4.1}$$

Where k'_{mn} is the cut off wave number of the cylindrical waveguide, χ'_{mn} is the eigenvalue of the cylindrical waveguide system and it is 2.405 for the TM_{01} mode as the root of the Bessel function for TM_{mn} mode dispersion relation, f'_c is the cut off frequency of the cylindrical waveguide and c is the light speed in the vacuum.

Now the guiding beam radius of an electron [Swati, Chauhan and Jain (2016)] is given as-

$$r_b = \frac{\chi'_{mn\pm h,i} R_{dt-FEL}}{\chi'_{mn}} \tag{4.2}$$

Where the radius of the electron beams is r_b, i is the beam radial positions (i.e., 1 or 2) and the harmonic number is h, always $h \geq 1$. In the amplifier interaction chamber, the RF wave is extracted out from the beams electron of slow wave space charge through the forward propagation with group velocities in positive direction and leaving out the RF signal at the output port, however, the negative group velocities are also available here with backward waves propagation into the interaction region [Swati, Chauhan and Jain (2016)]. And the electron beam energy E_b is depends upon the beam voltage V_o of the electrons and define by $\gamma_o = [1 + E_b / m_e c^2]$ or $\gamma_o = [1 + V_o(kV)/511]$. Here γ_o is the relativistic time dilation factor associated with the total kinetic energy E_b of the electron beams.

The transportation of the beam from the source to the interaction region is a big issue, hence, the wigglers play an important role to the transportation of the beams into the interaction chamber in FELs. There are two kinds of wigglers, one is a permanent magnetic wiggler in which have essentially an arrangement of magnets is called a linear wiggler or planner wiggler and second is a circularly polarized wiggler or helical wiggler. Therefore, the permanent magnets can place on top in x-axis and underneath on the y-axis, then produce a wiggler magnetic field as [Freund and Antonsen, Jr. (2018), Marshall (1985), Tripathi (2013)],

$$\overline{B}_w = B_w(\hat{x} + i\hat{y})e^{ik_w z} \tag{4.3}$$

Where k_w is the wiggler number and B_w is the wiggler amplitudes of the vector potential for wiggler field and these two components are out of phase by $\pi/2$, this is called

circularly polarized wiggler, hence, the wiggler magnetic field in x-direction is $B_w \cos k_w z$ and $B_w \sin k_w z$ in y-direction and the equations one obtains as,

$$\overline{B}_w = B_w[\hat{x}\cos(k_w z) + i\hat{y}\sin(k_w z)] \tag{4.4}$$

A wiggler with a strong uniform magnetic field (B_w) providing the negative-mass effect is proposed and designed for this experiment with the axial guiding magnetic field (B_o) . The consideration of the ponderomotive force by the relativistic equation of motion for electron beams is define as the rate of change of momentum [Balal et al. (2015)], i.e.,

$$\frac{d}{dt}\overline{P} = -\frac{e}{c}\overline{v}_{ob} \times (B_o \hat{z} + \overline{B}_w) \tag{4.5}$$

Where momentum $\overline{P} = m_e \gamma_o \overline{v}$, $\gamma_o = (1 - v_{ob}^2 / c^2)^{-1/2}$ is relativistic gamma factor or Lorentz factor for electrons, m_e is the rest mass of the electron and c denotes speed of light in vacuum and , $\overline{v}_{ob}$ is the drift velocity of electrons.

Now for launch a circularly polarized amplifiers radiation through the length of $z = 0$ end with electric field [Marshall (1985), Liu and Tripathi (1994), Tripathi (2013)] i.e.,

$$\vec{E}_L = A_L(\hat{x} + i\hat{y})e^{-i(\omega_L t - k_L z)}. \tag{4.6}$$

Where the radiation wave number of the amplifiers, $k_L = \omega_L / c$ and frequency of radiation, $\omega_L >> \omega_p, \omega_c$. It imparts oscillatory velocities to beam and plasma. If radiated electrons

move with a whistler wave, then the phase matching condition at (ω, k), $\omega = \omega_L - \omega_w$ and $k = k_L + k_w$ to be satisfied as [Freund and Antonsen, Jr. (2018), Liu and Tripathi (1994)],

$$v_{ob} = \frac{\omega}{k} = \frac{\omega_L - \omega_w}{k_L + k_o}. \tag{4.7}$$

Since $k_L = \omega_L / c$ and $v_{ob} \approx c$, this equation gives [Freund and Antonsen, Jr. (2018), Marshall (1985), Liu and Tripathi (1994)],

$$\omega_L \approx 2\gamma_o^2 k_w c = 2\gamma_o^2 \omega_w, \tag{4.8}$$

or,
$$\lambda_L \cong \lambda_w / 2\gamma_o^2. \tag{4.9}$$

Here equation (4.7) used for designing of wiggler size and interaction lengths of the FEL amplifiers. And this results in a broad tunability that permits the free-electron laser to operate across virtually the entire electromagnetic spectrum. If the wiggler period is shorter, then the radiation frequency is become shorter. This reduces wavelength of radiation by increasing the electrons beam energy. In the term of total γ_o is written as $\lambda_L = \frac{\lambda_w}{\beta_b(1+\beta_b)\gamma_o^2}$ at $\beta_b = v_b / c$. It is also written as $\lambda_L = (\frac{\lambda_w}{2\gamma_o^2})(1 + \frac{a_w^2}{2})$, where $a_w = \frac{eB_w\lambda_w}{2\pi m_e c^2} = 0.9337 B_w \lambda_w$ is called wiggler constant or wiggler parameter [Freund and Antonsen, Jr. (2018), Roberson (1989), Pellegrini (1990)]. The wiggler field B_w is expressed in Tesla and the wiggler period λ_w is in centimeters.

Since an electron streaming in the axial direction, therefore, experiences a transverse force and acquires a transverse velocity component upon entry into the wiggler. Hence, the transverse wiggler velocity (v_w) is proportional to the product of the wiggler amplitude and period. This relationship may be expressed as [Freund and Antonsen, Jr. (2018)],

$$\frac{v_w}{c} = -\frac{a_w}{\gamma_o} \tag{4.10}$$

Since the motion is circular in a helical wiggler, both axial and transverse velocities have a constant magnitude. This is important because the resonant interaction depends upon the axial velocity of the beam. In addition, the wiggler induces a constant-magnitude transverse velocity (v_w), with the relation between the total electron energy and the streaming energy. As a result, the resonant wavelength depends upon the total beam energy, the wiggler amplitude and period through the relation as,

$$\lambda_L \cong \frac{\lambda_w}{2\gamma_o^2}(1 + a_w^2) \tag{4.11}$$

It is the interaction between the transverse wiggler-induced velocity with the transverse magnetic field of an electromagnetic wave that induces a force normal to both in the axial direction. This is the ponderomotive force. An electron in near resonance with the ponderomotive wave lose energy to the wave, if their velocity is slightly greater than the phase velocity of the wave and gain energy at the expense of the wave in the opposite case.

In contrast, a solenoidal field has a deep and subtle effect on the interaction mechanism. This arises because a solenoidal field results in a precession, called Larmor rotation, about the magnetic field lines that can resonantly enhance the helical motion induced by the wiggler. This enhancement in the transverse velocity associated with the helical trajectory occurs when the Larmor period is comparable to the wiggler period. Since the Larmor period varies with beam energy, the relationship can be written as [Freund and Antonsen, Jr. (2018)],

$$B_o = 1.07 \frac{\gamma_o}{\lambda_w} \tag{4.12}$$

For fixed beam energies, therefore, this resonant enhancement in the wiggler-induced velocity requires progressively higher solenoidal fields as the wiggler period is reduced. The stabilization of the axial size of the bunch (which is required to provide the coherent character of the radiation) is due to the negative-mass instability (NMI) of the motion of the bunch through a long operating wiggler. Since, the wiggler-induced transverse velocity (v_w), hence, it is written as,

$$v_w = \frac{\omega_w v_\parallel}{\omega_o - k_w v_\parallel} \tag{4.13}$$

Where $v_\parallel$ is the electron axial velocity, $\omega_w = eB_w / \gamma_o m_e c$ is the wiggler frequency and the electron cyclotron frequency is $\omega_o = eB_o / \gamma_o m_e c$. In contrast to the orbits in the absence of an axial magnetic field, the presence of the axial field establishes a preferred direction of propagation through the wiggler in which propagation parallel to the axial field results in an

enhancement in the transverse velocity. The constants which determine the transverse and axial velocities are related through the requirement that the energy is conserved; hence

$$v_w^2 + v_\parallel{}^2 = (1-\gamma_o^{-2})c^2 \tag{4.14}$$

One effect of the axial solenoidal field is to resonantly increase the magnitude of the transverse wiggler-induced velocity when the Larmor period associated with the axial field is comparable to the wiggler period (i.e., $\omega_o \approx k_w v_\parallel$). The radius of the helical wiggler (r_w) motion about the orbit center of helix is measured with $r_w = v_w / k_w v_\parallel$ while expression $\lambda_w = r.k_w$ is represent the orbit radius of the electron motion with the center of drift tube of the FEL amplifiers [Freund and Antonsen, Jr. (2018)].

4.2.2. RF Interaction modeling

The FEL amplifiers is designed undulator/wiggler to performing wiggle array of the RF interaction behavior in CST particle studio for particle-in-cell (PIC) simulation as shown in Fig. 4.2 (flow chart), as designed parameters described in Table 4.1, Table 4.2 and Table 4.3. Fig 4.2, shows the Flow chart for PIC simulation of the FEL amplifiers in the TM_{01} mode, which has been helped us to study the eigen mode analysis and the simulation techniques and their results has been also analyzed with 3D particle-in-cell (PIC) codes “CST particle studio”. The modeling and designing of RF interaction chamber, there are various parameters used as wiggler, magnetic fields, gap size between magnets and wiggler periods, cylindrical waveguide with specific radius, drift tube, beams and beams radius, lengths of interaction chamber, operating frequency and S-parameters and so on.

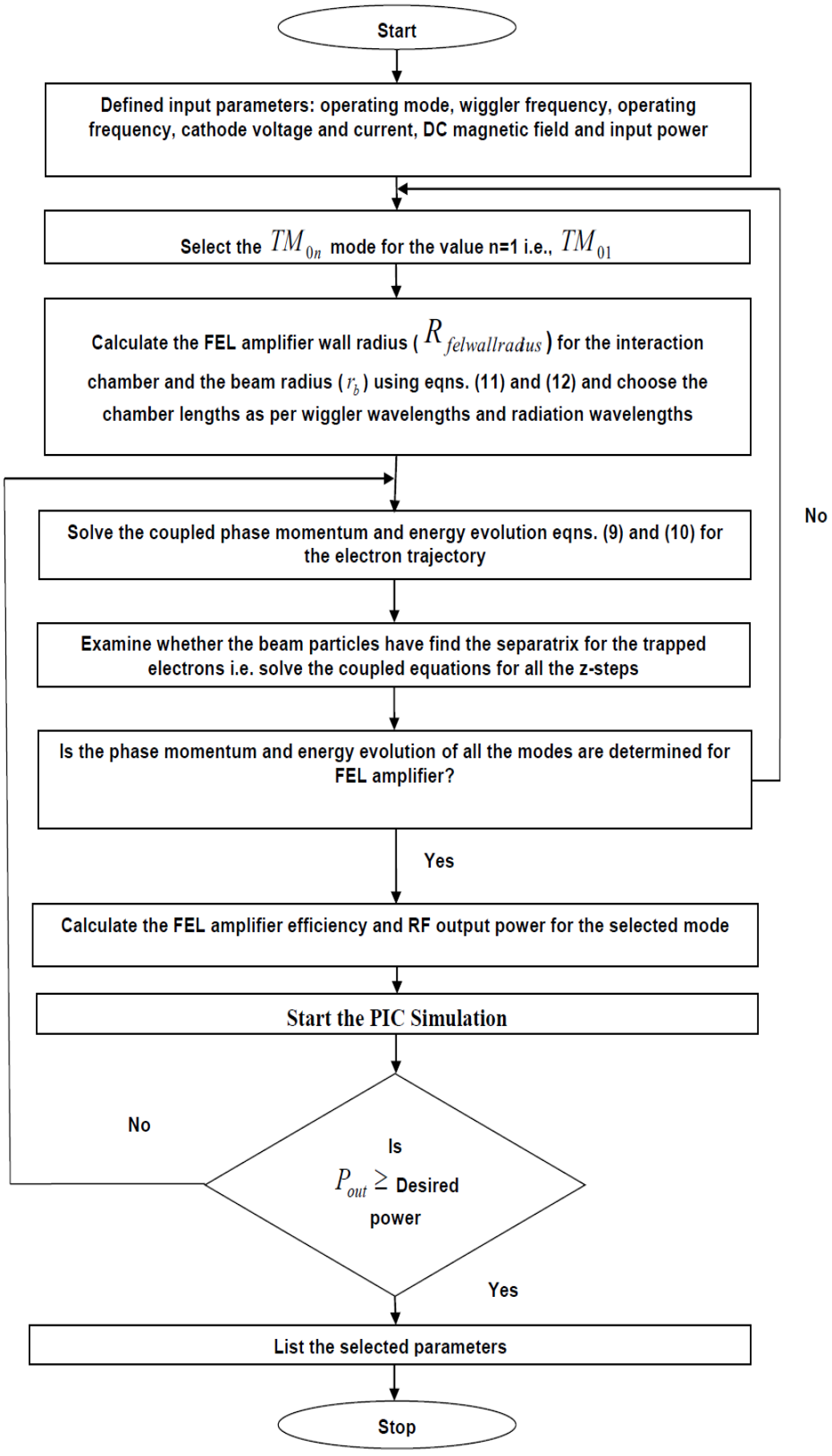

Figure 4.2: Flow chart of design procedure of the FEL amplifiers [Gopal and Jain (2018)].

The wiggler structure is modeled with iron magnetic materials (NdFeB) and vacuum background set. The drift tube is loaded with lossy dielectric materials to achieving the optimized s-parameters and allows adjusting of the amplifier behavior. Also the electric field (E-field) monitor is adjusting to ensure the electric fields through the input port and the observation of desired mode and their operating frequency is examined. On other hand, the magnetic field (H-field) monitor is set to observe the calculation of s-parameters which provide the complete isolation between the interactions chambers of both ends by observing the field leaked inside the interaction chamber. The phenomenon of the energy transferred from electrons to beat-wave ensured by setting the bunch formation of electrons through the phase space monitor.

Table 4.1
Design wiggler parameters of the FEL amplifiers (231GHz)
[Gold *et al*. (1984), Pant and Tripathi (1994)]

Magnetics wiggler parameters	**Values**
Wiggler wavelengths (λ_o)	$30mm$
Wiggler magnets size	$3\times3\times11mm^3$
Gap size	$12mm$
Wiggler frequency (f_o)	$10GHz$
Wiggler fields (B_o)	$3kG$
No. of poles (N)	21
Interaction Lengths (L)	$630mm$

Table 4.2
Design beam parameters of the FEL amplifiers (231GHz)
[Gold *et al*. (1984), Pant and Tripathi (1994)]

Electron beams parameters	**Values**
Wave guide type	Uniform cylindrical
Wave guide radius $(R_{felwallradus})$	$5.5mm\ (outer)$ $5.4mm\ (inner)$
Transverse mode	TM_{01}
Wave guide cut off frequency (f_c)	$21.27GHz$
Beam radius (r_b)	$3mm$
Bunch energy (E_b)	$1.25MeV$
Beam current (I_b)	$1kA$
Pulse duration (t_b)	$50n\sec$

Table 4.3
Design radiation parameters of the FEL amplifiers (231GHz)
[Gold *et al*. (1984), Pant and Tripathi (1994)]

Radiated output parameters	**Values**
Collective regime frequency	66-90 GHz
Radiation wavelengths (λ_1)	$1.2796mm$
Radiation frequency (f_1)	$231.2GHz$
Relativistic Gamma Factor (γ_{ob}^{o})	3.4
Axial guide fields (B_s)	$Up\ to\ \ 20kG$
Longitudinal momentum spreading $(P_{\|})$	0.1%
Output Power (P_o)	$50MW$

To foreclose the negative group velocities, which is propagate in the backward wave direction, the oscillation frequency of the device is greater than the cut off frequency of the cylindrical wave guide which is used into the amplifiers. The detailed design procedure and flow chart of the FEL amplifiers (FELA) is given Fig. 4.2 and the listed data given in Table 4.1, Table 4.2 and Table 4.3.

4.3. Device Simulation

Fig. 4.1 (a), shown a typical lay out in 2-D and Fig. 4.1 (b & c), represented 3-D design schematics of a FEL amplifiers which consist of e-gun/accelerator, cathode, cylindrical waveguide, modulating interaction chamber, undulator/wiggler as magnetic arrangement, axial magnetic fields, depressed collector for beam collection and finally optical mirror to collect the FEL amplifiers radiated output. The interaction chamber is mainly used to phase bunching phenomenon and implementation of beam modulation techniques between wiggler magnetic fields to electron beams which produces beat-wave excitation as ponderomotive waves. In order to understanding the mechanism of beam-wave interaction and performance analysis of the FEL amplifiers are designed and simulated through the commercial PIC simulation using "CST particle studio" [*User's Manual, CST-Particle Studio* (2014), Kartikeyan, Borie and Thumn (2004)]. The FEL amplifier is modeled as Fig. 4.1 (a, b & c), as per the material property, magnetic field, electric field and designed parameters as listed in Table 4.1, Table 4.2 and Table 4.3.

The performance analysis of EM simulation in Eigen mode (i.e., beam-absent analysis or cold analysis) is examined to secure the operating mode field stimulation and oscillating frequency and so on. In the last the device is excited in the supervision of beams

electron (i.e., hot analysis) to examine the frequency of operation, extraction efficiency, RF power output and gain. The amplifier design methodology and simulation techniques using PIC simulation codes "CST particle studio" is given below in details.

4.3.1. Eigen Mode Simulation

The Eigen mode simulation (i.e., beam absent simulation) is performed to assure the observation of the device in the desired mode and frequency using listed data in Table 4.1, Table 4.2 and Table 4.3. The Eigen mode solver in "CST particle studio" is used for the cold simulation to carry out its EM behavior between input into the RF interaction region and their both input and output ports. At boundary condition into the interaction chamber, the tangential compound is become null (i.e., $\vec{E}_t = 0$). Fig. 4.3 (a, b, c, d & e) shows the contour plot and vector plot of the magnetic fields and electric fields inside the input port and out port into the interaction chamber of the FEL amplifiers, which clarify that there is zero variation in azimuthal and radial direction that is defined the operation of TM_{01} confirmation into the interaction chamber and same operating mode (i.e., TM_{01}) is coming out at the output port for linear amplification in the FEL amplifiers.

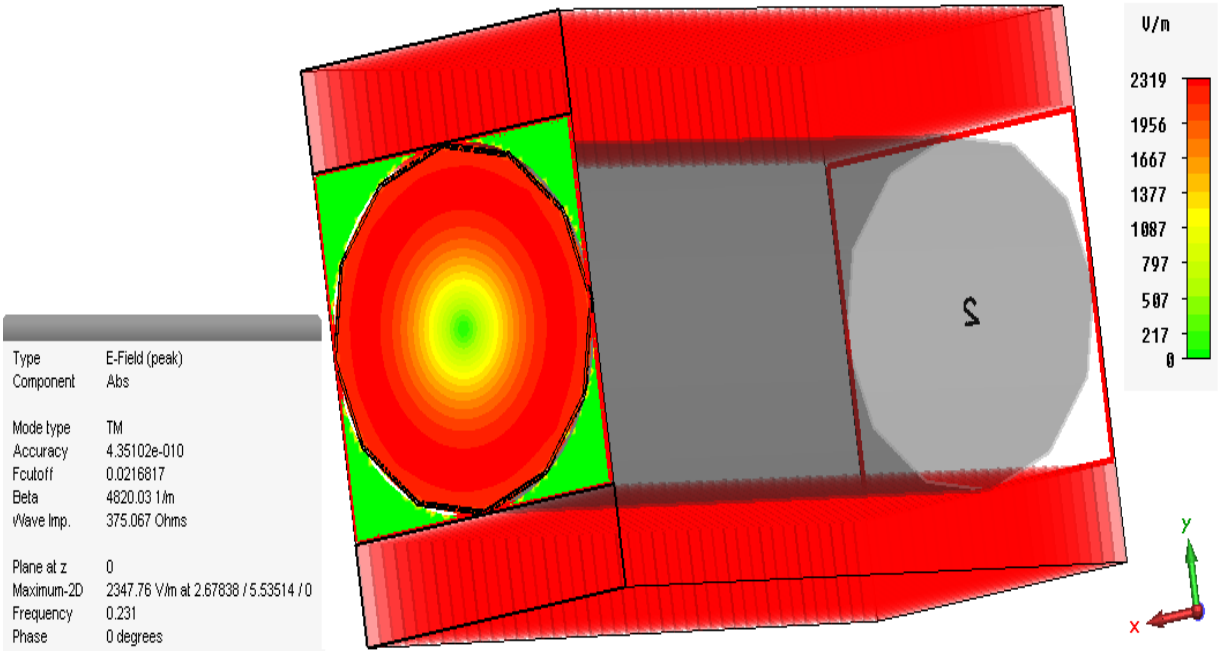
Type E-Field (peak)
Component Abs
Mode type TM
Accuracy 4.35102e-010
Fcutoff 0.0216817
Beta 4820.03 1/m
Wave Imp. 375.067 Ohms
Plane at z 0
Maximum-2D 2347.76 V/m at 2.67838 / 5.53514 / 0
Frequency 0.231
Phase 0 degrees
V/m
2319
1956
1667
1377
1087
797
507
217
0
y
x

(a)

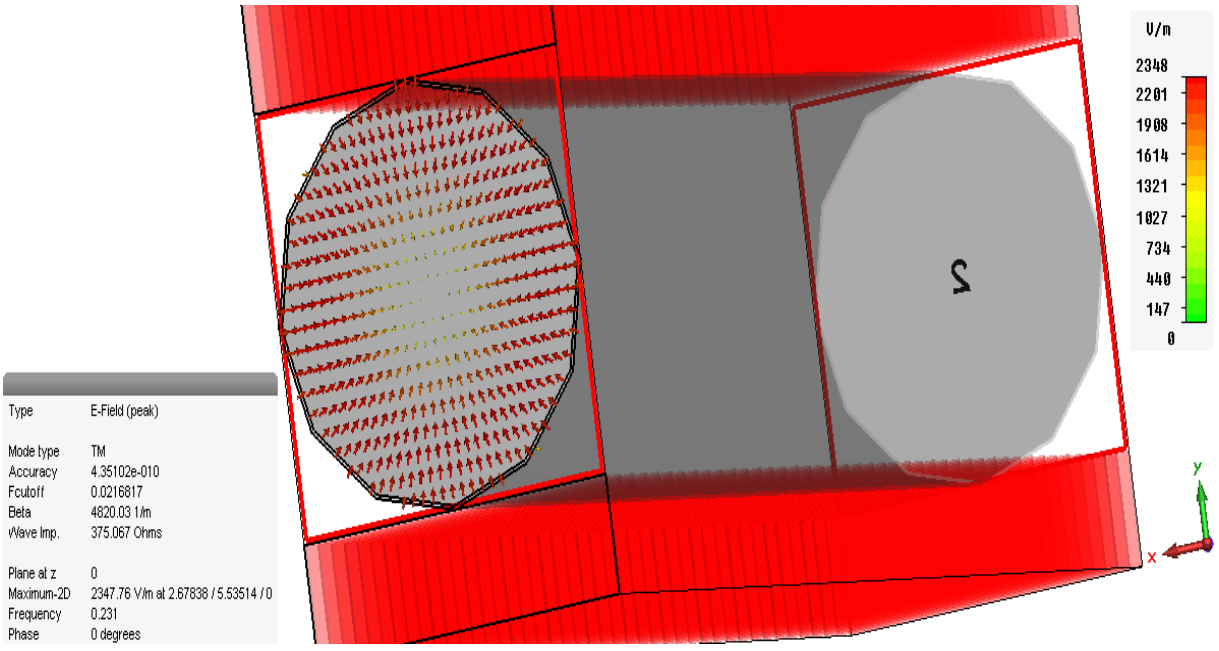
Type E-Field (peak)
Mode type TM
Accuracy 4.35102e-010
Fcutoff 0.0216817
Beta 4820.03 1/m
Wave Imp. 375.067 Ohms
Plane at z 0
Maximum-2D 2347.76 V/m at 2.67838 / 5.53514 / 0
Frequency 0.231
Phase 0 degrees
V/m
2348
2201
1908
1614
1321
1027
734
440
147
0
y
x

(b)

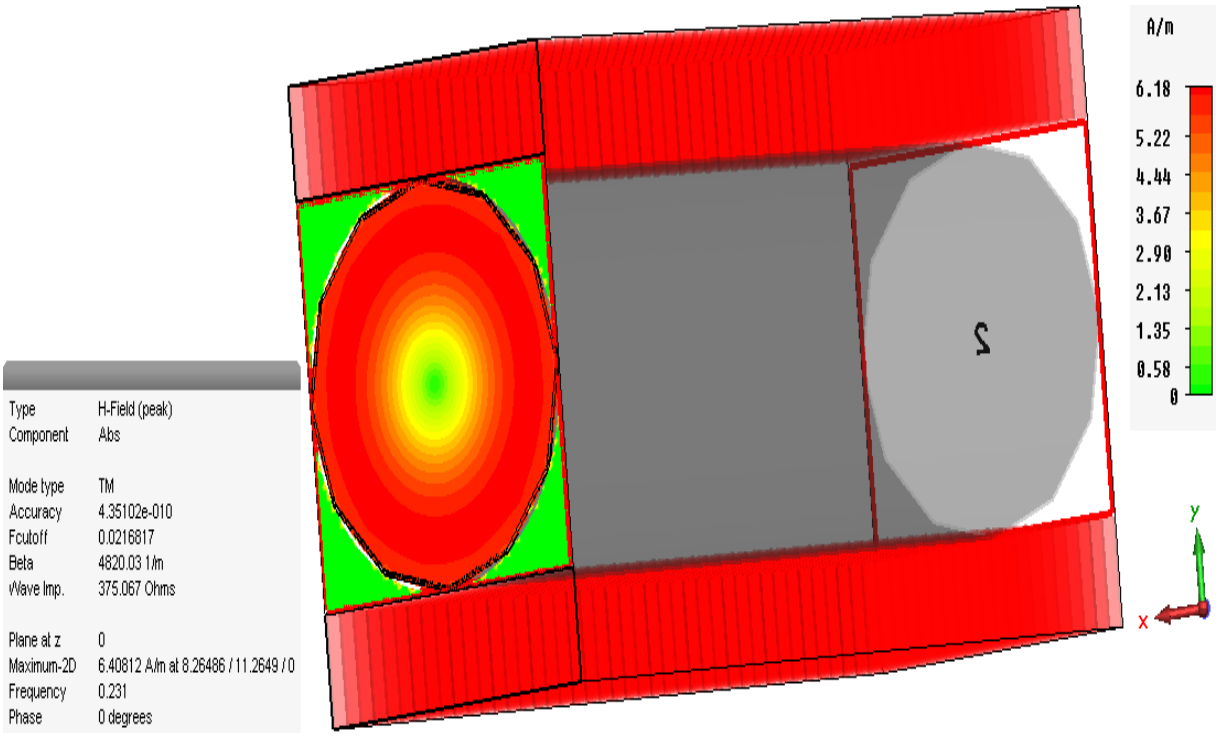
A/m
6.18
5.22
4.44
3.67
2.90
2.13
1.35
0.58
0
Type H-Field (peak)
Component Abs
Mode type TM
Accuracy 4.35102e-010
Fcutoff 0.0216817
Beta 4820.03 1/m
Wave Imp. 375.067 Ohms
Plane at z 0
Maximum-2D 6.40812 A/m at 8.26486 / 11.2649 / 0
Frequency 0.231
Phase 0 degrees
y
x

(c)

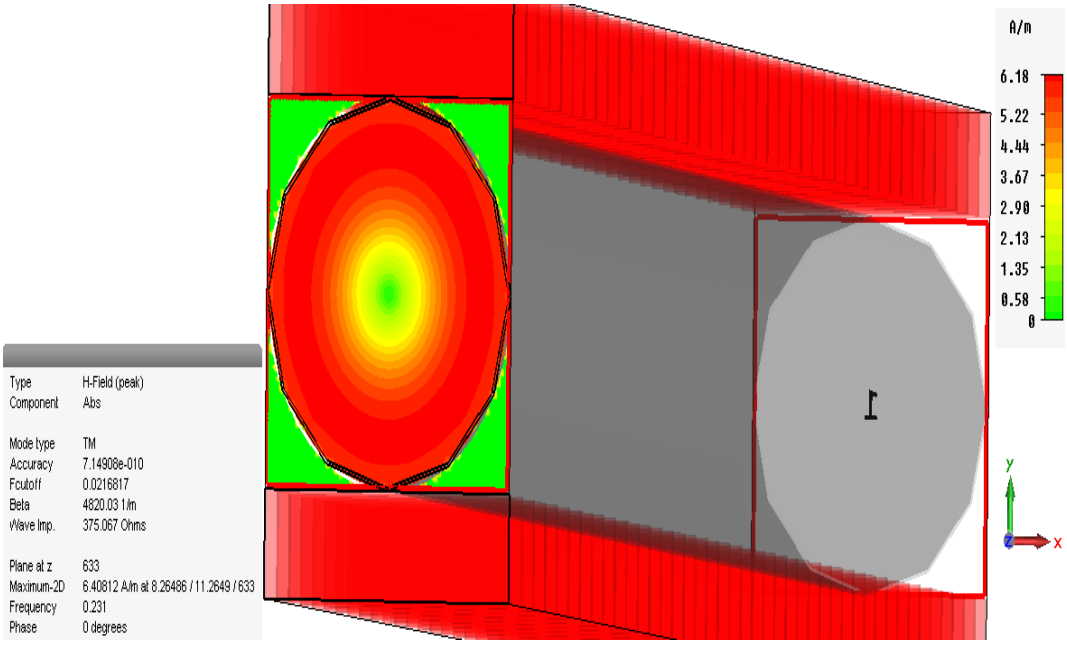
A/m
6.18
5.22
4.44
3.67
2.90
2.13
1.35
0.58
0
Type H-Field (peak)
Component Abs
Mode type TM
Accuracy 7.14908e-010
Fcutoff 0.0216817
Beta 4820.03 1/m
Wave Imp. 375.067 Ohms
Plane at z 633
Maximum-2D 6.40812 A/m at 8.26486 / 11.2649 / 633
Frequency 0.231
Phase 0 degrees
y
x

(d)

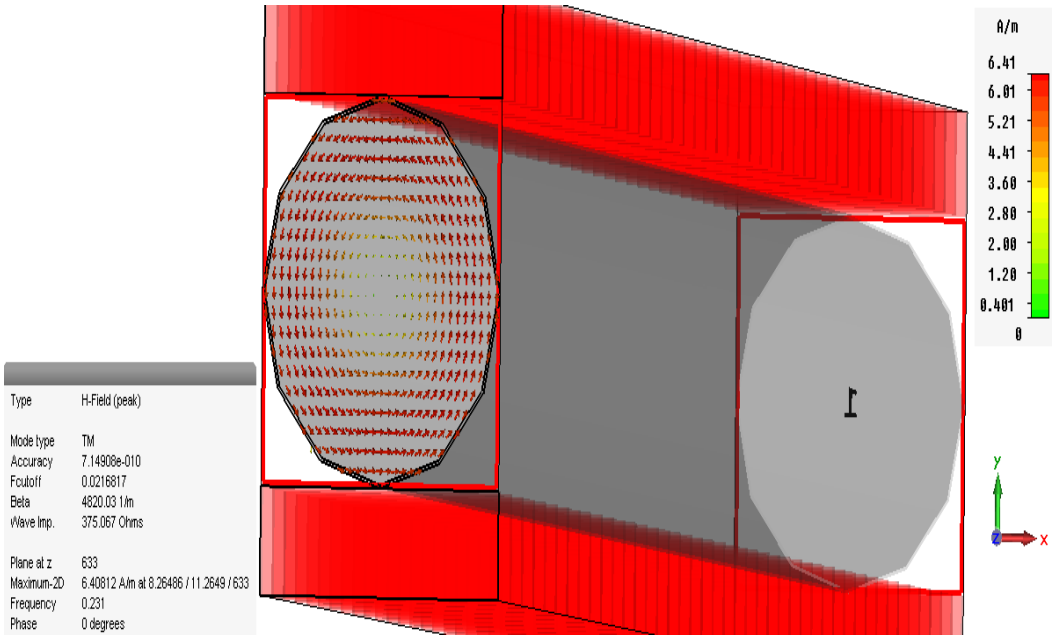

(e)

Figure 4.3: Fields pattern of the FEL amplifiers for the desired TM_{01} mode (i) Electric field patterns at the input port (a) contour plot (b) vector plot (c) Magnetic field patterns at the input port , contour plot, and (ii) Magnetic field patterns at the output port (d) contour plot and (e) vector plot.

In the Fig. 4.4 (a, b & c), the dielectric loss and s-parameters (the standard values of the s-parameters magnitude is varied between $-30dB$ to $-180dB$) calculation is readily available through the 3-D/2-D field processing and as a results shown in the given figure for the specific parameters and dominant mode $S_{21} \rightarrow S2(3),1(3)$, which is shows the availability of the device. And also sustain the accepted power in Watts.

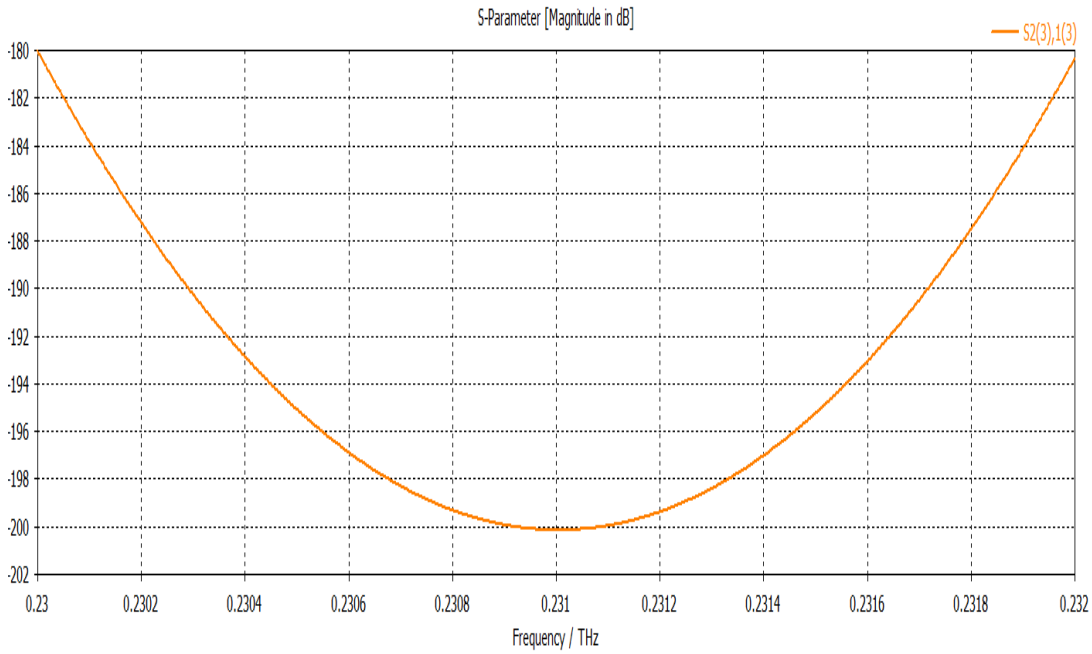
S-Parameter [Magnitude in dB]
S2(3),1(3)
-180
-182
-184
-186
-188
-190
-192
-194
-196
-198
-200
-202
0.23
0.2302
0.2304
0.2306
0.2308
0.231
0.2312
0.2314
0.2316
0.2318
0.232
Frequency / THz

(a)

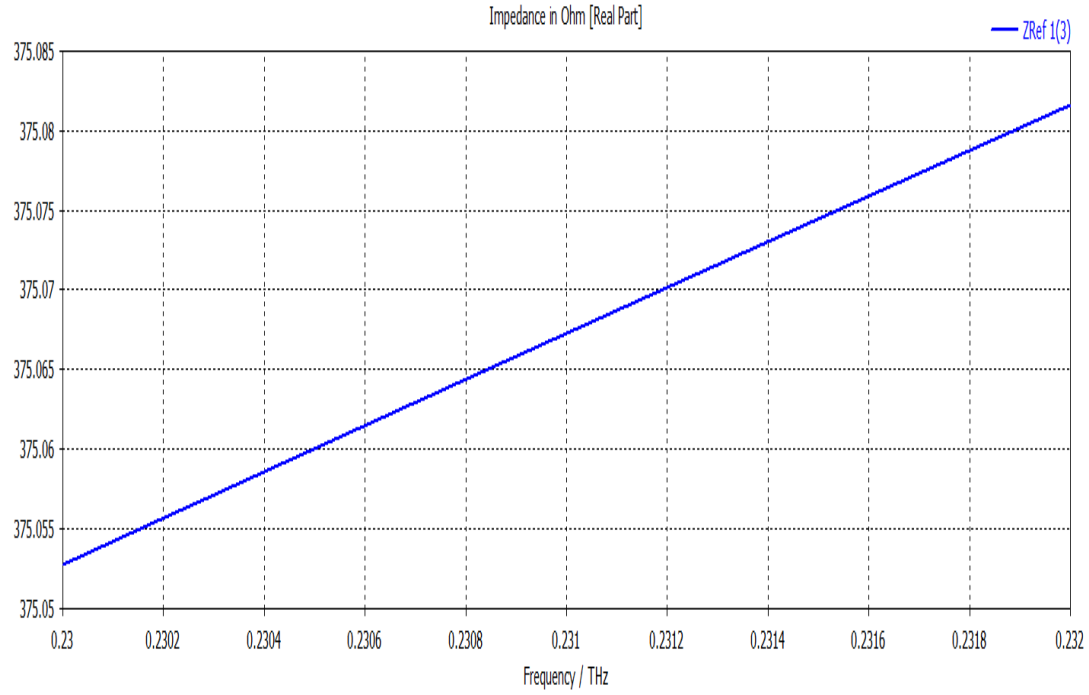
Impedance in Ohm [Real Part]
ZRef 1(3)
375.085
375.08
375.075
375.07
375.065
375.06
375.055
375.05
0.23
0.2302
0.2304
0.2306
0.2308
0.231
0.2312
0.2314
0.2316
0.2318
0.232
Frequency / THz

(b)

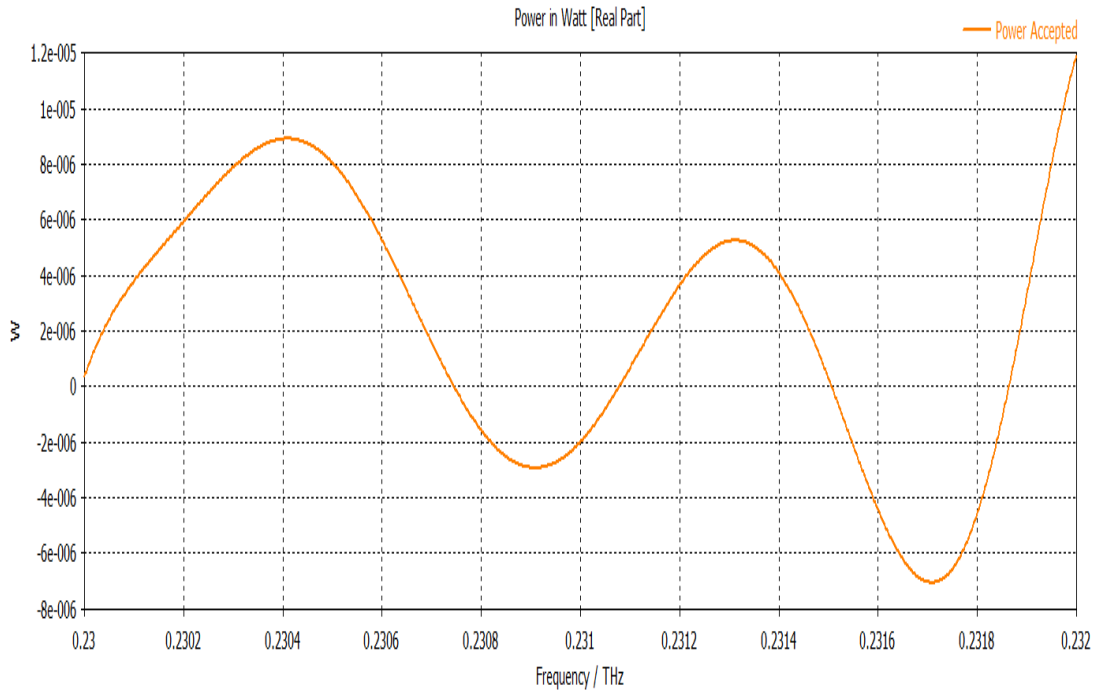

(c)

Figure 4.4: FEL amplifiers simulated and desired observation for (a) S-parameters (b) Impedance in Ohm (c) Power accepted.

4.3.2. Parametric Analysis

The parametric analysis of the free electron laser amplifiers (FELA) is estimated by using the particle-in-cell (PIC) simulation in "CST Particle studio" to study the device sensitivity for the various parameters of the beams. The efficiency variation and RF output power has been estimated to the different frequencies radiation. Fig. 4.5 shown the RF power output of the FEL amplifier is increases after increasing the taper axial magnetic

fields (B_s). The overall the phenomenon of the extraction efficiency is increases of the amplifiers.

The magnetic field values are as 1.6 Tesla for uniform while 1.74 Tesla used for linear tapering respectively. Tapering of the magnetic field is a crucial role to enhance the efficiency of the net transfer energy of the wave, which is estimated as 20% achievable efficiency than that of the 5% for uniform FEL amplifiers [Pant and Tripathi (1994)]. It is also higher than experimentally demonstrated the high power FEL amplifiers (FELA) using relativistic electron beams (REBs) at *35GHz* for *1.2dB/cm* growth rates and estimated an experimental efficiency *>3%* with 50dB gain for uniform amplifiers while examined an effect of tapering on axial magnetic field to enhance the efficiency and power of the device that indicate the production of *>75MW* at *75GHz* with experimental efficiency of *6%* [Gold *et al.* (1984)].

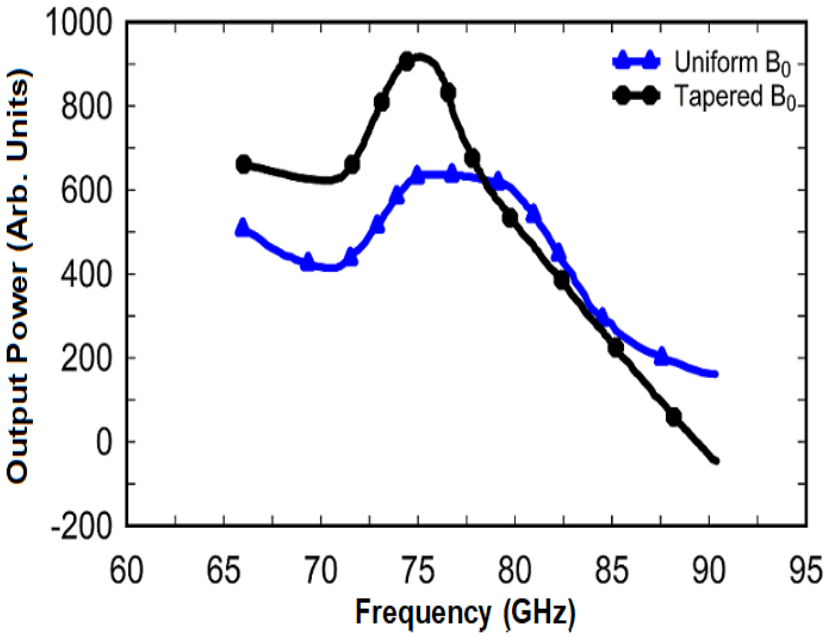

Figure 4.5: FEL amplifiers output power vs radiated frequencies [Gold *et al.* (1984)].

4.4. Result and discussion

Based on the analytical method, high power microwave- Free Electron Laser Amplifiers is studied. A computer friendly numerical code is written to analyze the beam-wave interaction mechanism in the Free Electron Laser Amplifiers. To validate the optimized Free Electron Laser Amplifiers design obtained by following the device design methodology, the PIC simulation results obtained by modeling the device through CST Particle Studio are validated with the analytical results.

4.4.1. Magnetostatic Analysis

The helical wiggler based on redistribution of magnetic field of a solenoid by different type of ferromagnetic helix has been explore in the present work and studied both in theory and CST simulation in beam absent case. Such wigglers are very simple and efficient for promising sources of coherent spontaneous radiation from dense electron bunches [Balal *et. al.* 2017]. According to beam absent simulations study, the development of negative-mass instability (NMI) in a combined strong uniform and helical wiggler fields can provide maintenance of nearly constant sizes of short and long-living bunch cores at a fairly large wiggler length and makes possibilities of the implementation of powerful and narrowband radiation sources. In contrast, in regimes of the negative mass stabilization (NMS), the coherent spontaneous emission is provided at the wiggler lengths. This leads to a significant enhancement in both the power and the duration of the radiated pulse, whereas the radiation frequency is lower than in the regime with the zero guiding field [Balal *et al.* (2015)]. For typical parameters of a THz source (particle energy of 5 - 6 MeV, bunch charge of up to 1 nC, and radiation frequency of 1–2 THz), the value of wiggler field,

B_w should be of the order of 0.1–0.2 T, that is tens of times smaller than the guiding field, B_o [Balal 2017].

Correspondingly, a relatively thin steel helix is proposed to be sufficient for providing the required value of wiggler field, B_w. Let us find the field of a helical insertion placed into an infinite solenoid with a uniform field. Considering here, the magnetization $\bar{J}$ of an infinite ferromagnetic cross sectional view of helix with wiggler period λ_w, inner and outer radius 'r_1' and 'r_2', respectively, thickness t = r_2 – r_1, and axial size 'd' shown below Fig. 4.6. In the case of a very strong guiding field, the magnetization of the helix is saturated, $\bar{J} = \bar{J}_\infty$, so that its direction practically coincides with direction of the field, $\bar{z}_o$ and its value does not depend on B_o. The boundary conditions at the cylindrical surface $r = R$ (mean radius) correspond to continuity of the potential and easy to show the static wiggler magnetic field at the axis of the system is expressed as,

$$B_w = \frac{1}{\pi} k_w^2 tR \sin(k_w d/2) K_1(k_w R) \mu_o J_\infty \qquad (4.15)$$

Where μ_o is the permeability for the ferromagnetic materials and $K_1(k_w R)$ is McDonald constant for first order Bessel function. Maximum of the transverse field is achieved when the axial size of the helix is equal to half of its period i.e., $d = \lambda_w / 2$. Also, above equation is well applied for thin helices with round cross sections if one takes parameters 'd' and 't' equal to each other, so that $(d.t)$ corresponded to the square of the wire cross section, and 'R' equal to the helix mean radius, i.e., '$r = R$'.

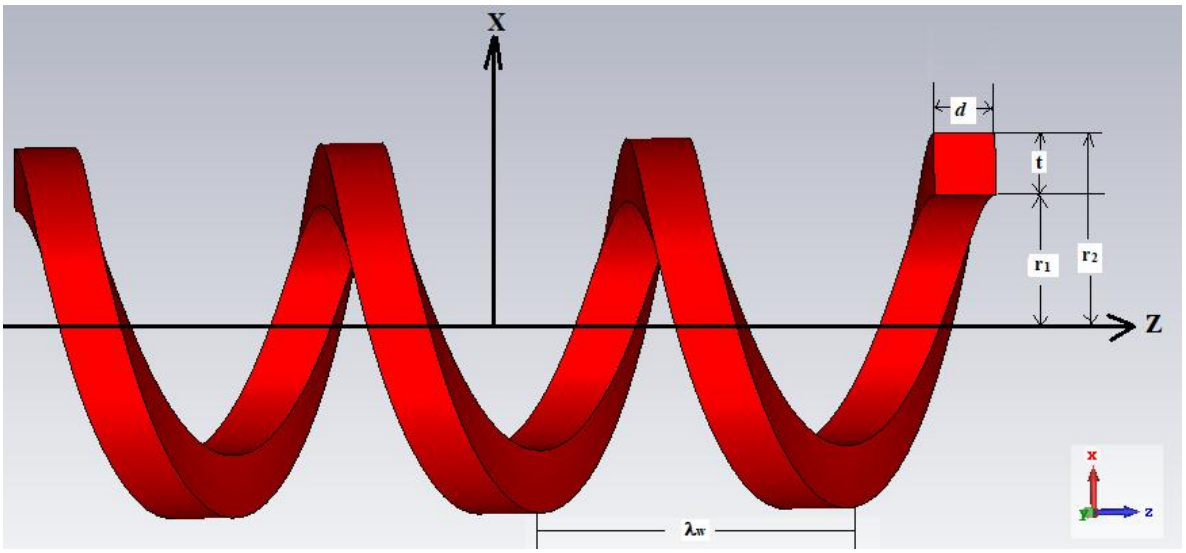

Figure 4.6: Cross sectional view of the helical wiggler

Equation (4.15) is validated with the help of magnetostatic solver equations using CST Particle Studio for partial re-distribution of transverse magnetic fields and axial magnetic fields amplitude with a finite thickness of the helix with rectangular cross section as well as round cross section with nonlinear permeability of Iron and Steel ferromagnetic materials [Balal *et. al.* 2017]. Simulation results of re-distributed transverse magnetic field amplitude $B_x(T)$ & $B_{\perp}(T)$ for the case of Iron helix and Steel helix with rectangular cross section and round cross section are shown in Fig. 4.7, Fig. 4.8, Fig. 4.9, Fig. 4.10, and Fig. 4.11. The parameters are as, (i) For rectangular cross section helix, wiggler period, λ_w=3 cm, inner radius of helix, r_1 =0.3 cm, outer radius of helix, r_2 = 0.5 cm, thickness of helix, t = $r_2 - r_1$ =0.2 cm, axial size of helix, *d*= 1.2 cm and magnetic fields B_w= 1.21 Tesla (ii) For round cross section helix, wiggler period, λ_w=3 cm, mean radius of helix, r =R_2= 0.55 cm,

outer radius of drift tube, R_2= 0.55 cm, inner radius of drift tube, R_1= 0.54 cm, wire radius of helix, r_w = 0.216 cm, center of wire with reference of wiggler center r_c= R_2+r_w = 0.766 cm and magnetic fields B_w= 1.6 Tesla.

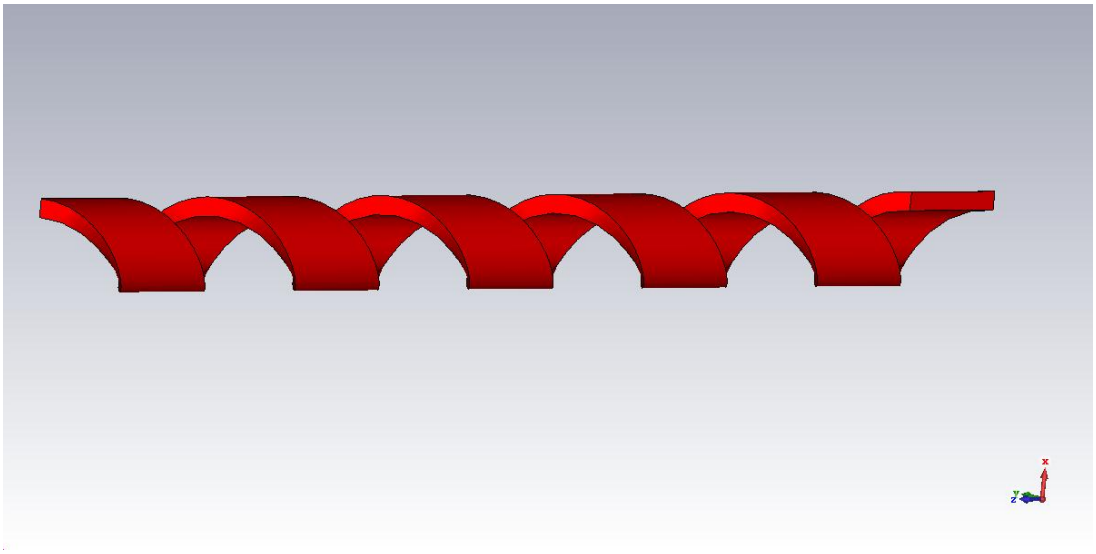

(a)

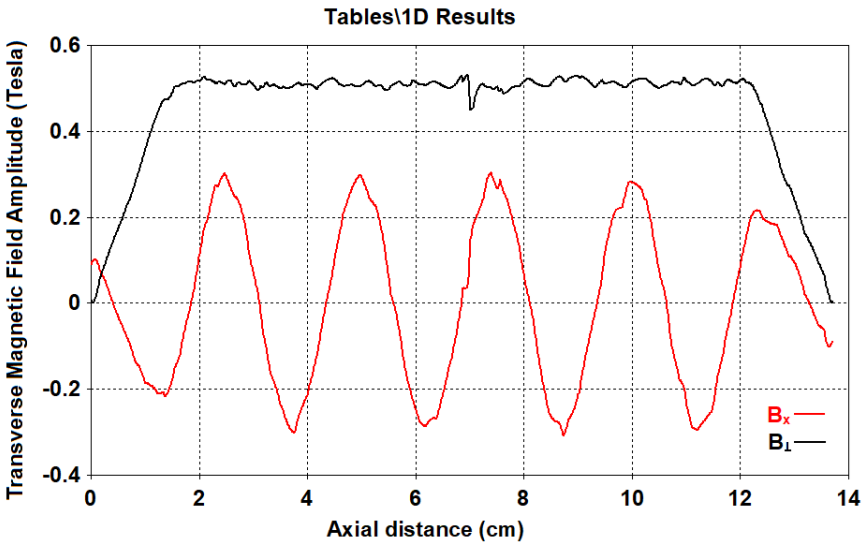

(b)

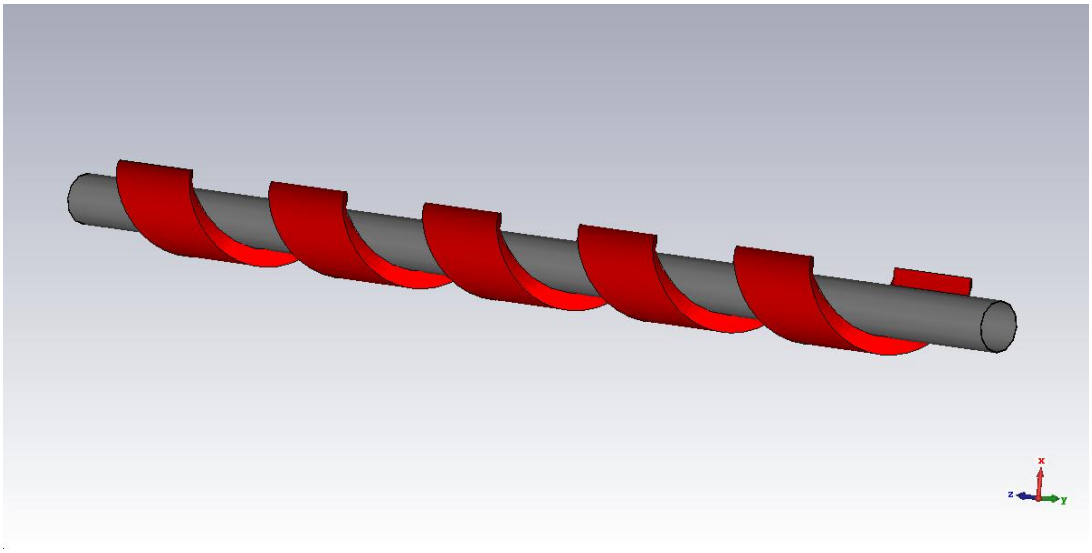

(c)

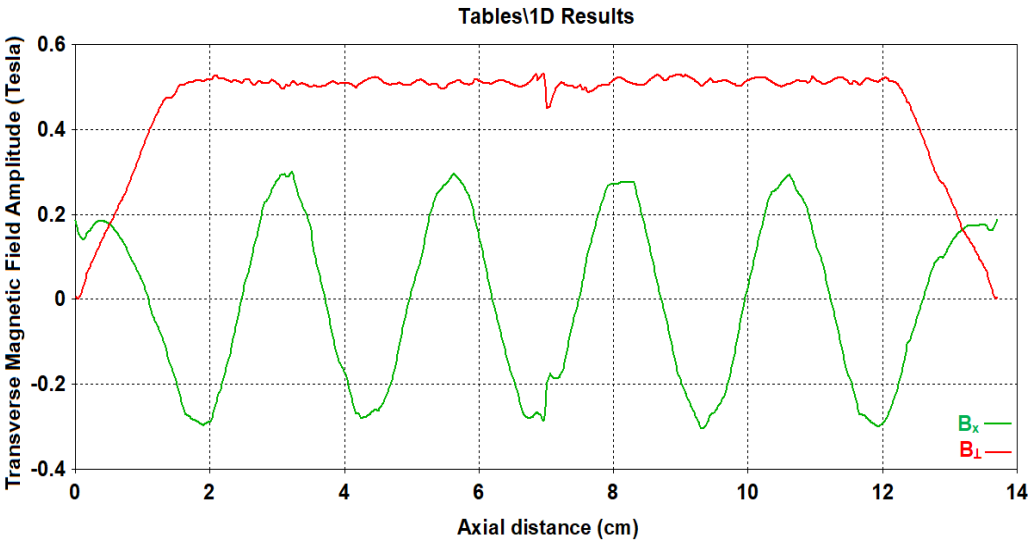

(d)

Figure 4.7: Simulation results for the case of **Iron helix** with rectangular cross section as (a) The helix geometry without drift tube (b) Transverse Magnetic Field Amplitude B_x (T) & B⊥(T) without drift tube (c) The helix geometry with drift tube (d) Transverse Magnetic Field Amplitude B_x (T) & B⊥(T) with drift tube.

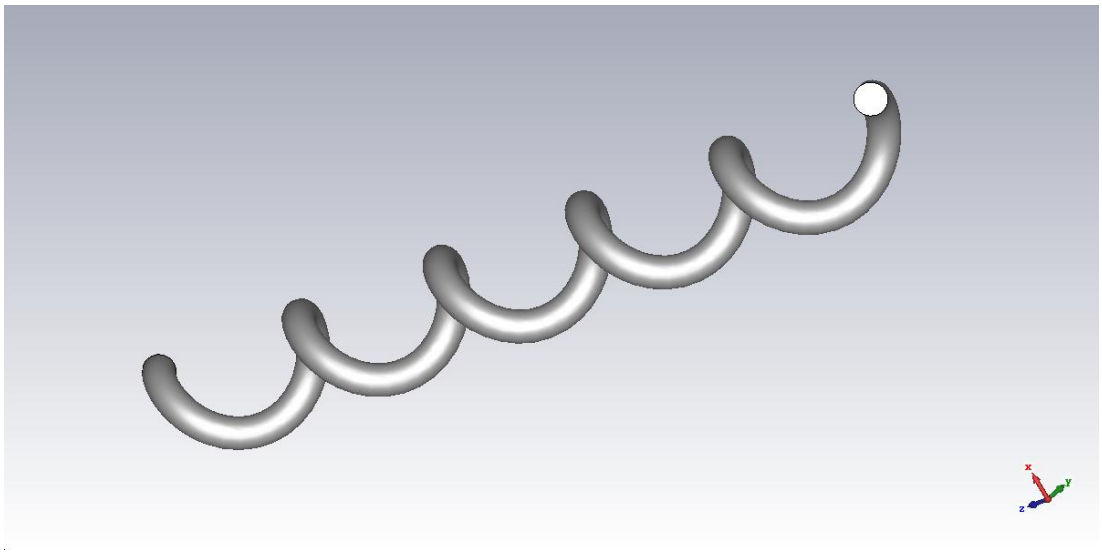

(a)

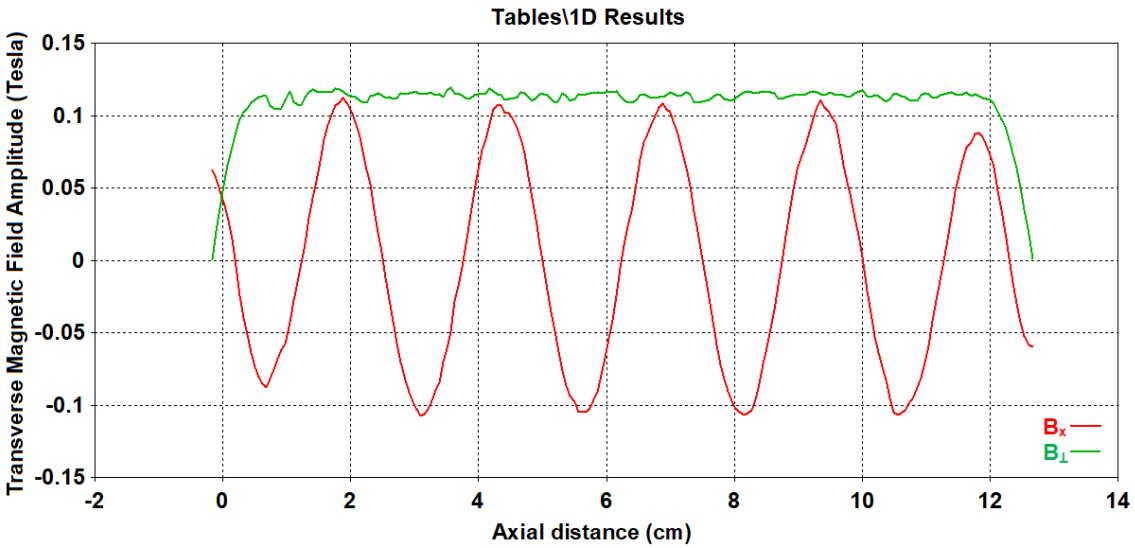
Tables\1D Results
Transverse Magnetic Field Amplitude (Tesla)
0.15
0.1
0.05
0
-0.05
-0.1
-0.15
-2
0
2
4
6
8
10
12
14
Axial distance (cm)
Bx
B⊥

(b)

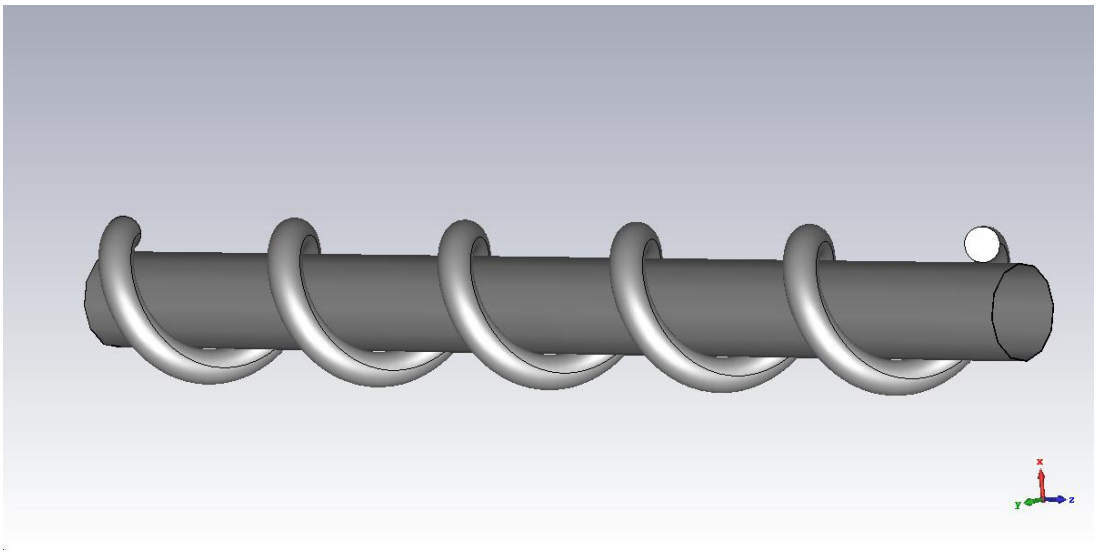

(c)

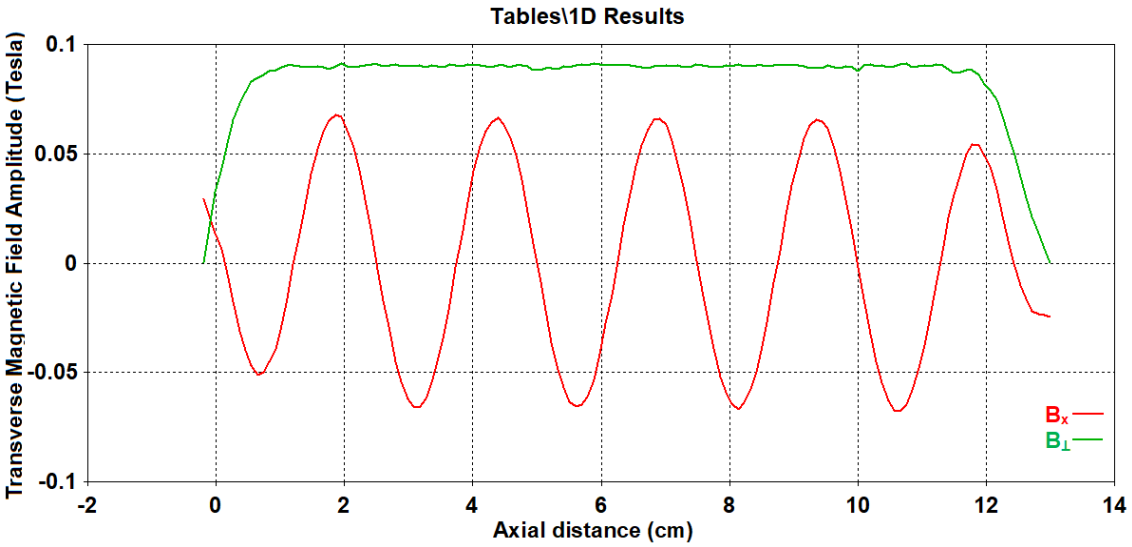
Tables\1D Results
Transverse Magnetic Field Amplitude (Tesla)
0.1
0.05
0
-0.05
-0.1
-2
0
2
4
6
8
10
12
14
Axial distance (cm)
Bx
B⊥

(d)

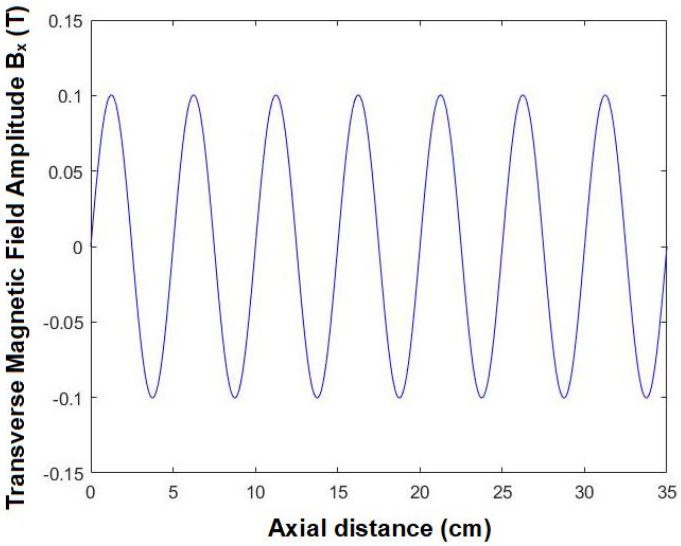

(e)

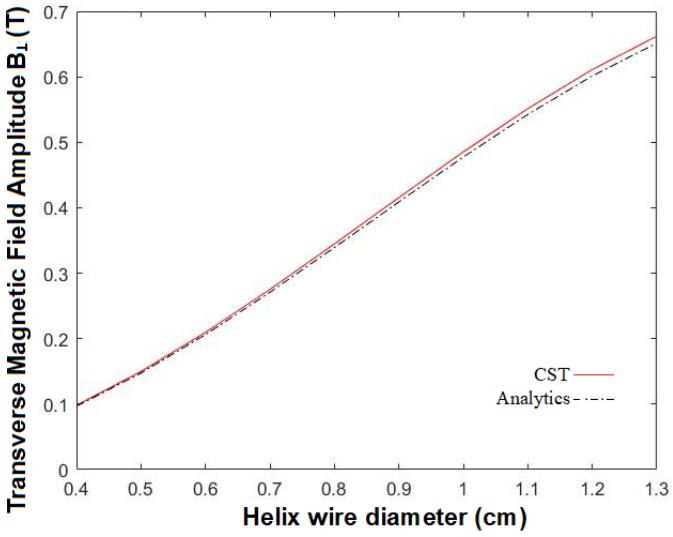

(f)

Figure 4.8: Simulation results for the case of **steel helix** with round cross section as (a) The helix geometry without drift tube (b) Transverse Magnetic Field Amplitude B_x (T) & $B_\perp$(T) without drift tube (c) The helix geometry with drift tube (d) Transverse Magnetic Field Amplitude B_x (T) & $B_\perp$(T) with drift tube (e) Transverse Magnetic Field Amplitude B_x(T) with drift tube (f) Transverse Magnetic Field Amplitude $B_\perp$(T) with helix wire diameter and The predictions of formula (4.15) is also validated for square cross section as shown in (f).

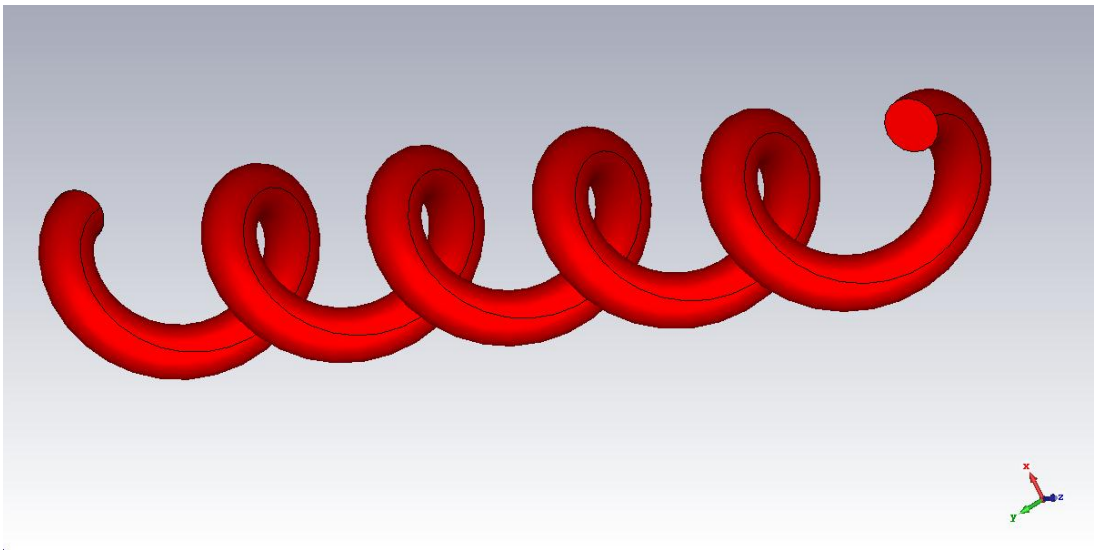

(a)

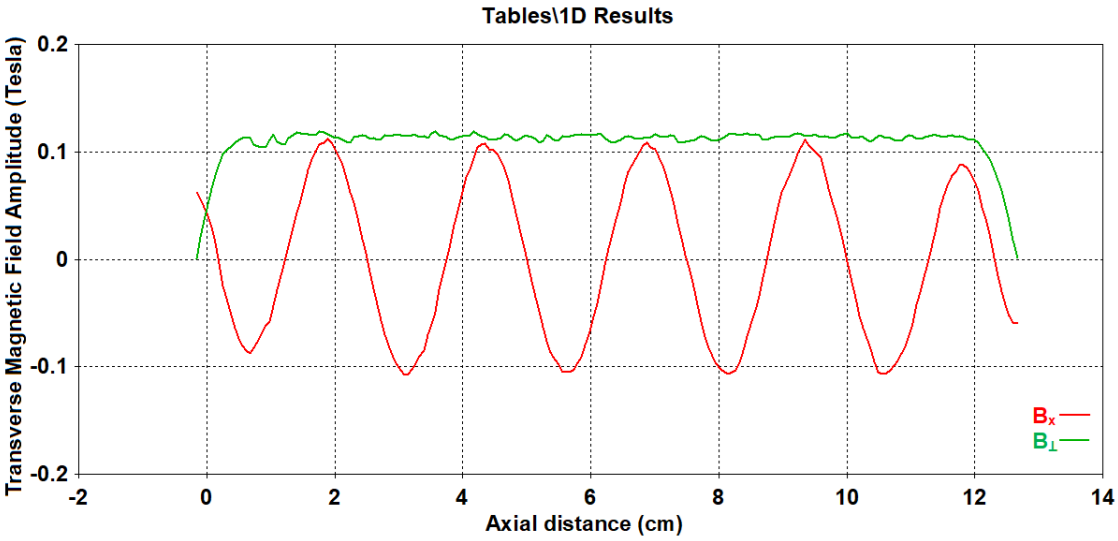
Tables\1D Results
Transverse Magnetic Field Amplitude (Tesla)
0.2
0.1
0
-0.1
-0.2
-2
0
2
4
6
8
10
12
14
Axial distance (cm)
Bx
B⊥

(b)

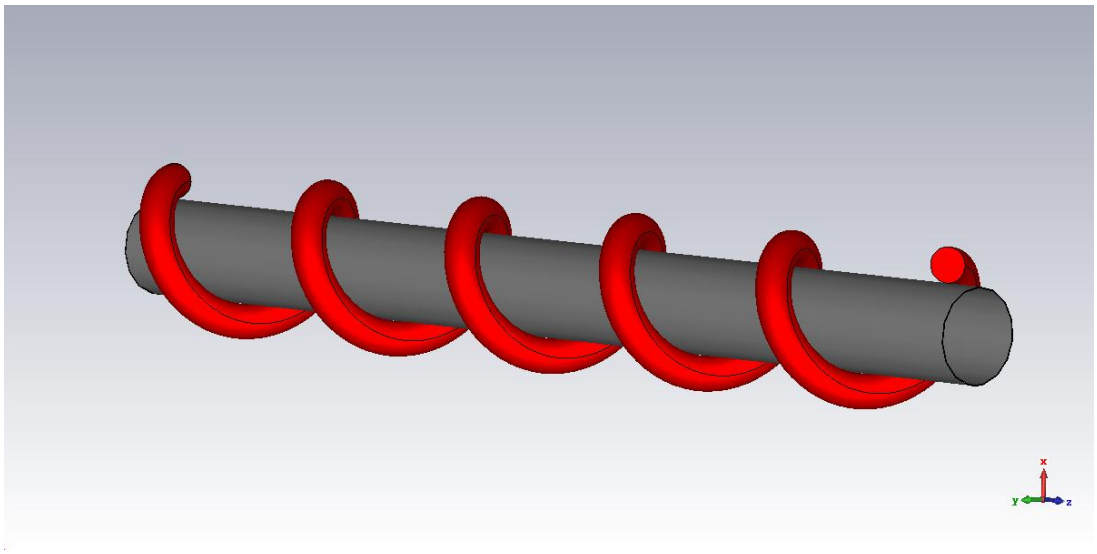

(c)

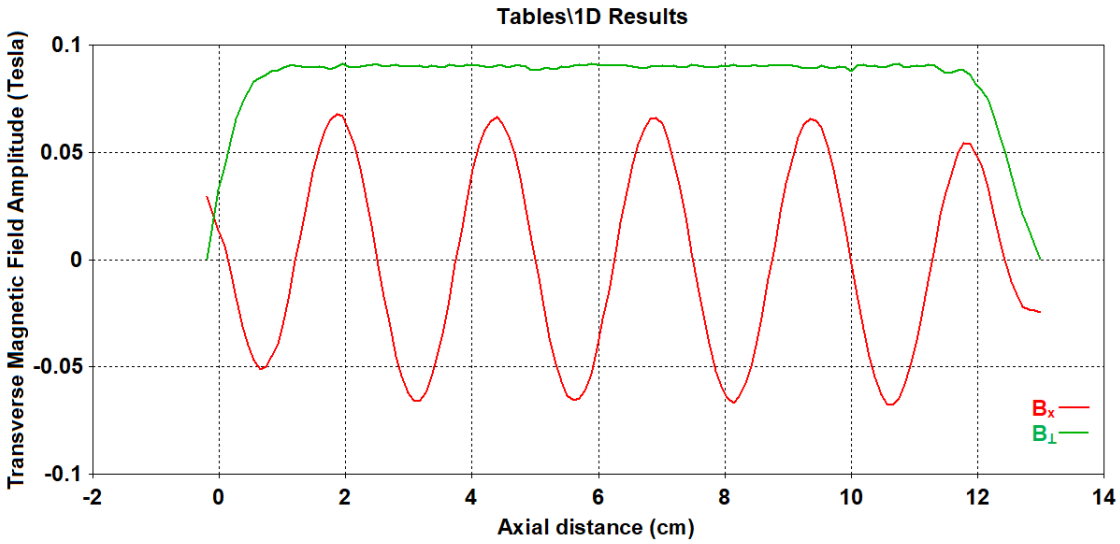

(d)

Figure 4.9: Simulation results for the case of **Iron helix** with round cross section as (a) The helix geometry without drift tube (b) Transverse Magnetic Field Amplitude B_x (T) & $B\perp$(T) without drift tube (c) The helix geometry with drift tube (d) Transverse Magnetic Field Amplitude B_x (T) & $B\perp$(T) with drift tube.

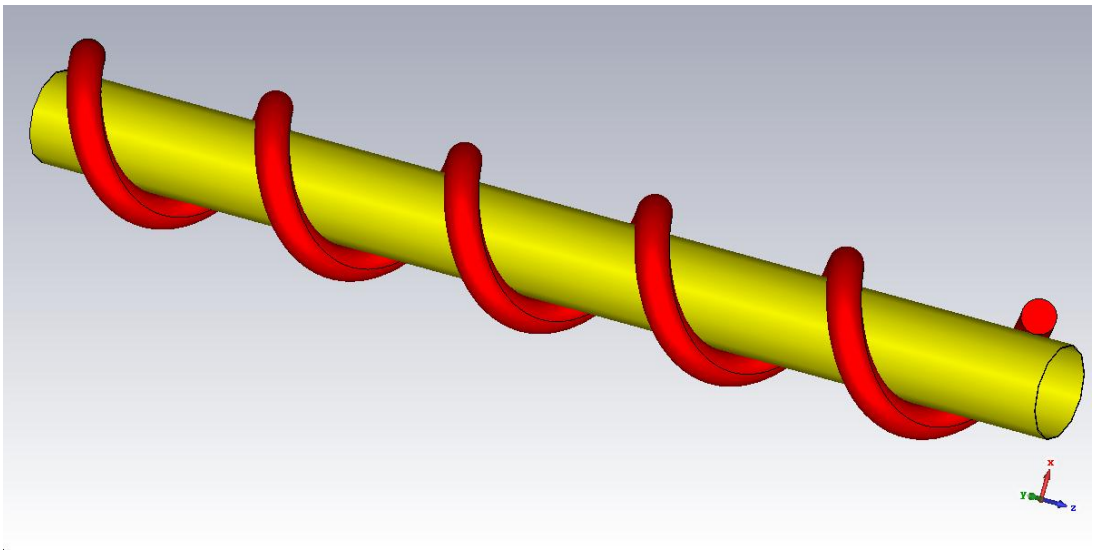

(a)

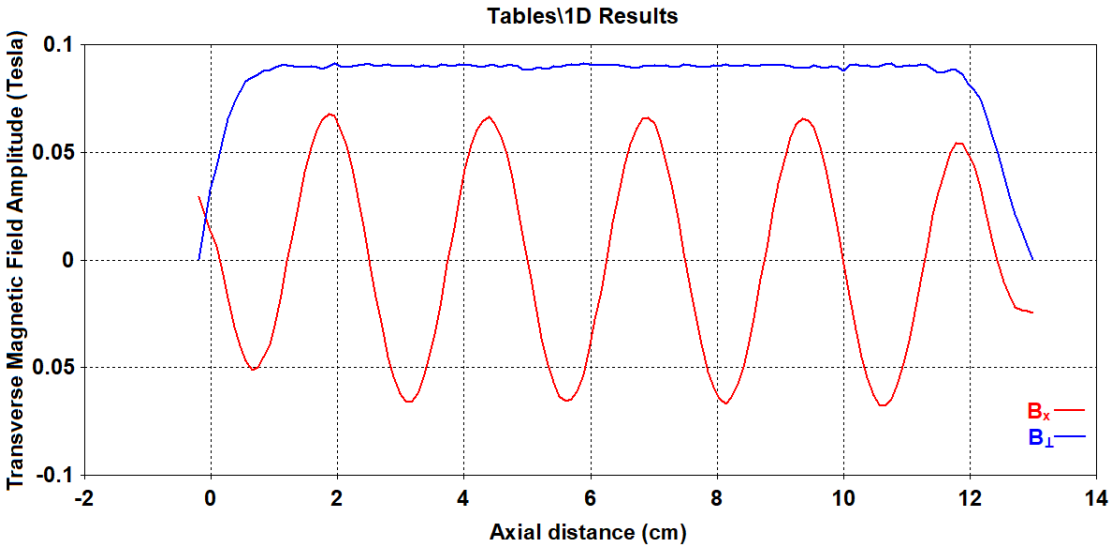

(b)

Figure 4.10: Simulation results for the case of **Iron helix** with round cross section as (a) The helix geometry with copper drift tube (d) Transverse Magnetic Field Amplitude B_x (T) & $B\perp$(T) with copper drift tube.

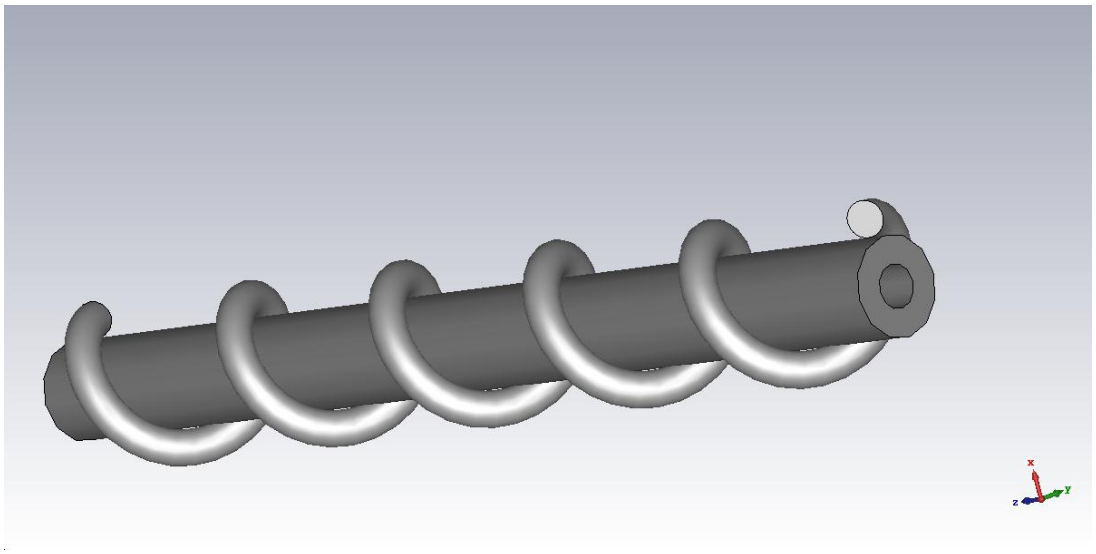

(a)

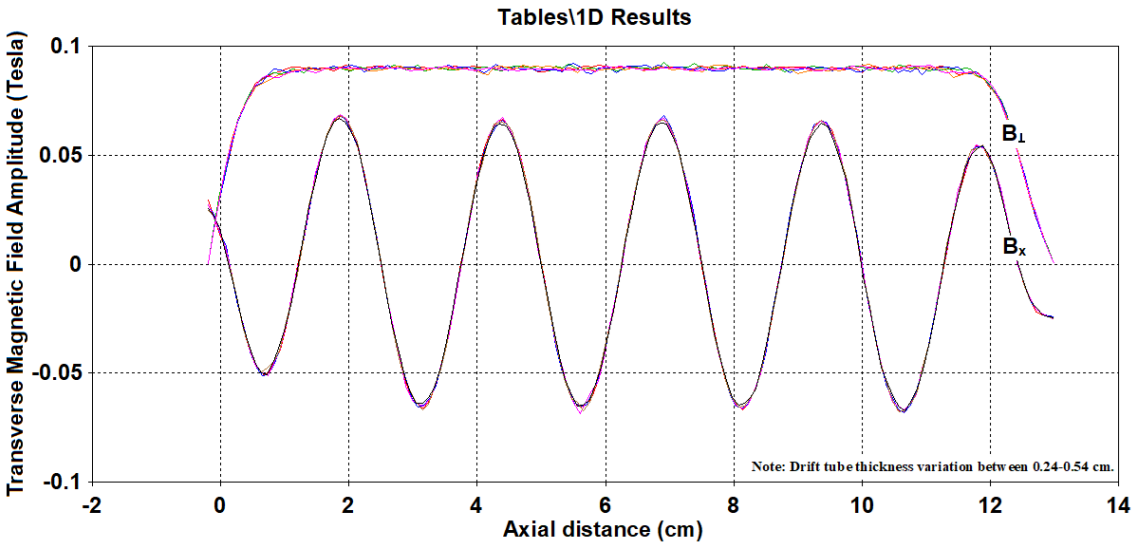

(b)

Figure 4.11: Simulation results for the case of **steel helix** with round cross section and drift tube thickness variation as (a) The helix geometry (b) Transverse Magnetic Field Amplitude B_x (T) & $B_\perp$(T) with drift tube thickness variation.

4.4.2. PIC Simulation

After performing the beam-absent simulation study, the PIC simulation is presented here to extend for the beam-present case. Further, for the PIC simulation in beam present case, electrons have been considered as uniformly distributed in drift tube with electron bunch forms and also their evolution along the axial direction with helical wiggler has been observed in time domain. In order to facilitate the simulation process, the space charge effect on the electron beam has been neglected. The electron beam energy of 164.99 keV with beam voltage of 164.99 kV, and beam current of 103.04 A, 60 ns pulse duration is exited in the input port of the device. The beam radius is taken 0.3 cm with 1% of velocity spreads. For round cross section helix wire, wiggler period, λ_w=3 cm, mean radius of helix, r =R=R_2= 0.55 cm, outer radius of drift tube, R_2= 0.55 cm, inner radius of drift tube, R_1= 0.54 cm, wire radius of helix, r_w = 0.216 cm, center of wire with reference of wiggler center r_c= R_2+r_w = 0.766 cm and wiggler magnetic fields B_w= 0.115 Tesla and axial magnetic fields (B_o) is 1.175 Tesla respectively. The bunch of electron beam interacts with self-consistently with the RF field present in the interaction chamber. A kinetic spread can be directly introduced into the beam to realize the more reasonable scenario with the axial velocity spread has been considered as 1%. Electrons start to make bunches along the RF interaction into the interaction chamber and interact with the RF field to the amplification of the FEL amplifiers. As a result, they transfer their energy to the RF wave in synchronism. This makes possible amplification of an electromagnetic wave at the cyclotron frequency of the FEL amplifiers shown in the Fig. 4.12 (a) (b) and (c) and the wiggling of electron bunches during beam present case PIC simulation are shown in Fig. 4.13 (a) & (b).

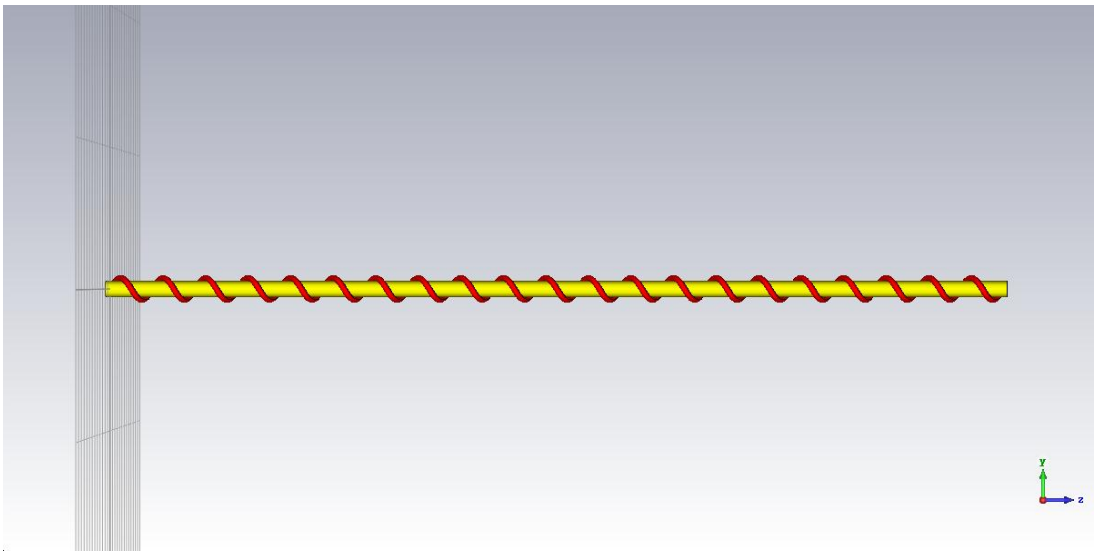

(a)

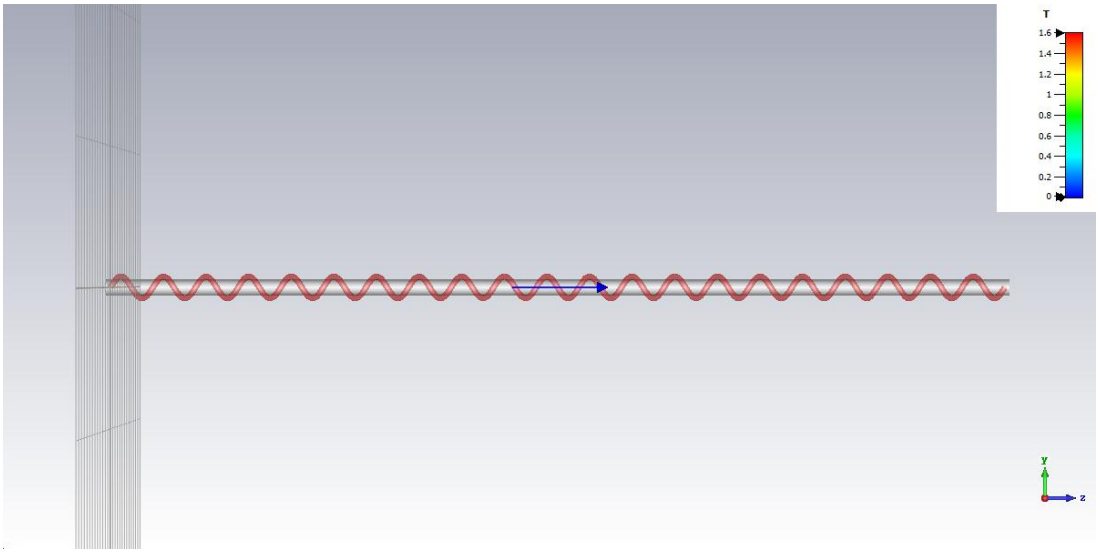

(b)

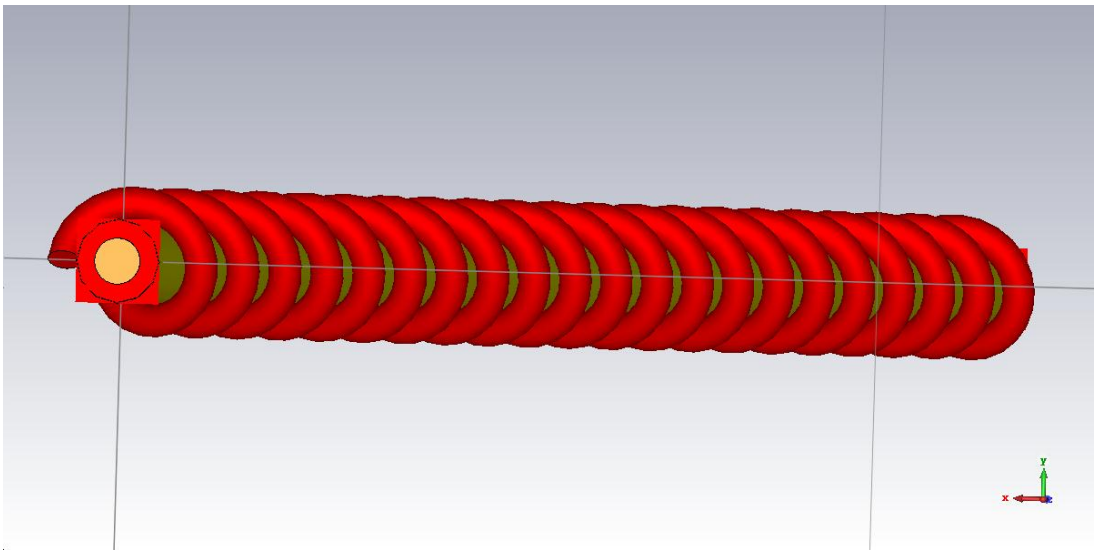

(c)

Figure 4.12: CST design model of FEL amplifiers (a & b) Lay out (c) diagram for simulation of the FEL amplifiers.

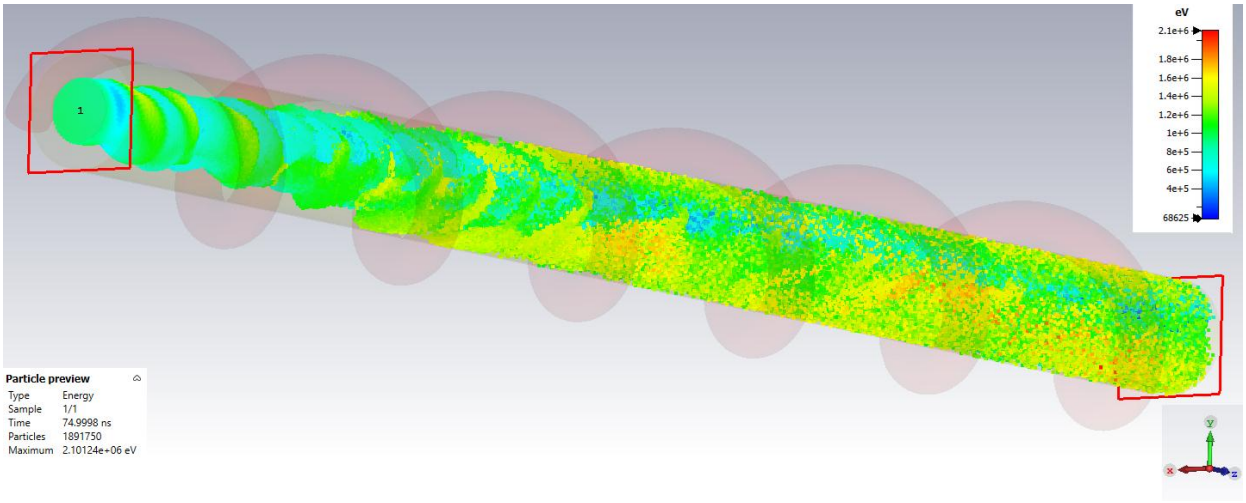

(a)

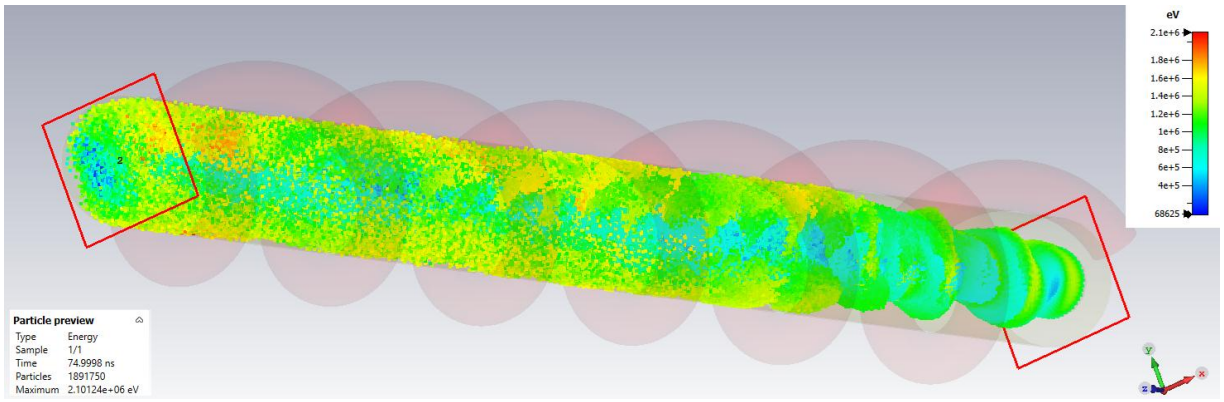

(b)

Figure 4.13: Wiggling view of the electron beams during PIC Simulations (a), & (b).

The power evolution of electron bunches transferred to the RF wave along the interaction region is shown in Fig. 4.14. It is noticed that initially all the electrons have the same energy of 164.99 keV but with time, the net energy of particles gets spreading along the interaction length of the device due to the interaction with the RF field. At the output end, majority of particles have lower energy which indicates the net energy transfer from the electrons to the RF wave, hence results in the amplification of the RF wave. To determine the operating frequency of the FEL amplifier, the frequency spectrum of the electric field amplitude is calculated which is obtained by taking the Fourier transform of the electric field as shown in Fig. 4.15. It is clear from the figure that the highest frequency peak is observed at around 35 GHz to TM_{11} mode, and hence therefore, confirms the frequency of operation of the FEL amplifiers.

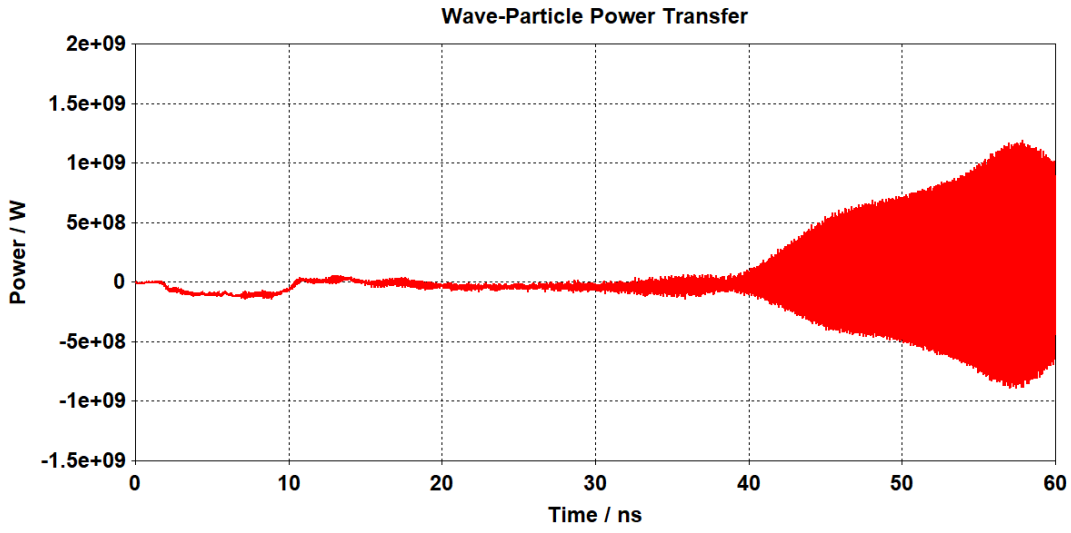

Figure. 4.14. Power evolution of the electron bunches transfer to the RF wave.

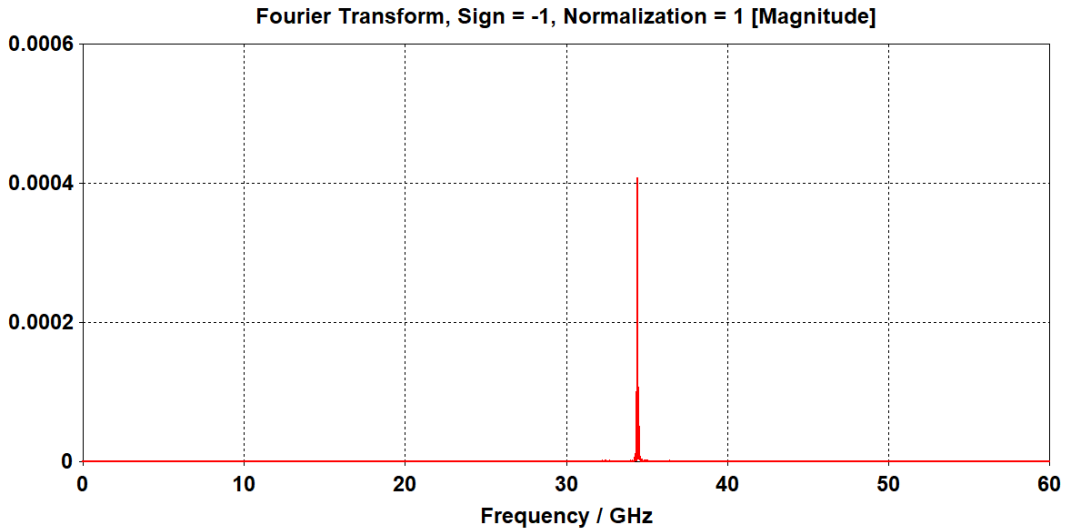

Figure 4.15: Frequency spectrum of the TM_{11} mode.

The temporal growth of the electric field amplitude in the TM_{11} mode operation is shown in Fig. 4.16. The output time signal corresponding to TM_{11} mode has the highest amplitude than all other modes at DC magnetic field B_0 = 1.175 Tesla with wiggler field (B_w) of 0.115 Tesla and the mode competition is mainly observed due to the fundamental harmonic TM_{01} mode. The growth of EM power approaches the saturation level at a time beyond 60 ns. After the template based post processing in CST particle studio, the saturated RF output power has been calculated as around 17 MW (Fig. 17) with an electronic efficiency of 20% for The electron beam energy of 164.99 keV with beam voltage of 164.99 kV, and beam current of 103.04 A, 100 ns pulse duration is exited in the input port of the device. The beam radius is taken 0.3 cm with 1% of velocity spreads. For round cross section helix wire, wiggler period, λ_w=3 cm, mean radius of helix, r =R=R_2= 0.55 cm, outer radius of drift tube, R_2= 0.55 cm, inner radius of drift tube, R_1= 0.54 cm, wire radius of helix, r_w = 0.216 cm, center of wire with reference of wiggler center r_c= R_2+r_w = 0.766 cm and wiggler magnetic fields B_w= 0.115 Tesla and axial magnetic fields (B_o) is 1.175 Tesla respectively.

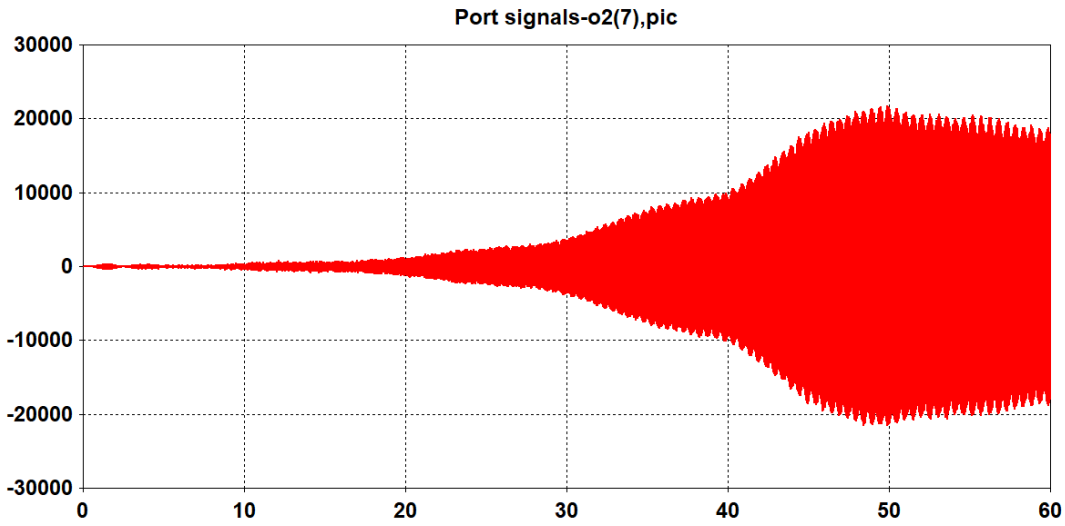

Figure 4.16: Temporal amplitude curve of the TM_{11} mode.

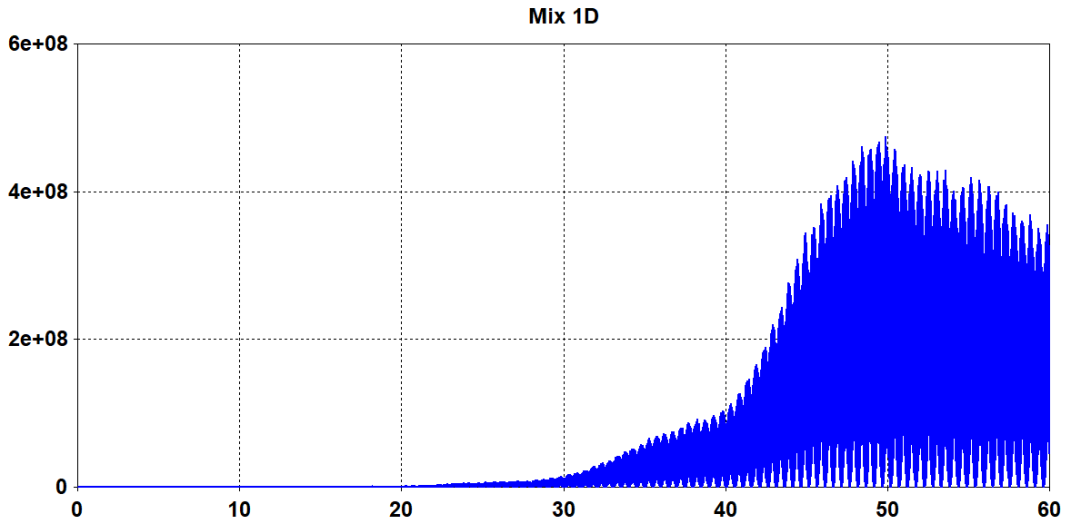

Figure 4.17: Temporal power plot of the TM_{11} mode.

4.5. Conclusion

The detailed description of the design methodology and results of simulation study of the highly radiated power microwave (HPM) device-FEL amplifiers has been presented. The FEL amplifiers show the simulated results as $50MW$ RF power output and 20% increases extraction efficiency with linear taper guided magnetic fields which is higher than that of experimental efficiency of >6% with 50dB gain [Gold *et al.* (1984)] for both end tapering and observed efficiency by 5% for an uniform FEL amplifies [Pant and Tripathi (1994)]. Therefore the device has been found a good agreement presented with $\approx 5\%$ experimental values as reported as previous paper and the overall performance of the FEL amplifiers has been spread, hence, the parametric analysis behavior through the particle-in-cell (PIC) simulation in "CST Particle studio" has been performed and validate. In this paper, the operating behavior and optimization in the TM_{01} mode of an FEL amplifiers has been discussed using the Eigen mode analysis and the simulation techniques and their results has been also analyzed with 3D particle-in-cell (PIC) code CST particle studio. To understand the performance analysis and sensitivity of the FEL amplifiers using IREBs on various parameter effects such as power, gain, efficiency, beam current, beam voltage and operating frequencies has been explained. In the modeling of an amplifiers, the pattern of the magnetic and electric field in TM_{01} mode has been showed and performed their RF simulation results in the absent case of electron beams i.e., the cold simulation. The reading of the measurement values has been showed for the large radiation growth rate 2dB/cm approximately with 231 GHz instantaneous band width. Additionally, the result to extraction of the kinetic energy from the electron beams to beat-wave has been observed the power and efficiency largely increases by 20% in the FEL amplifiers.